LBL-11516

Lawrence Berkeley Laboratory
UNIVERSITY OF CALIFORNIA

NOV 4 1981

FLUID DISTRIBUTION IN PROGRESSIVE PULMONARY EDEMA: A LOW TEMPERATURE SCANNING ELECTRON MICROSCOPY STUDY

Gregory Ross Hook
(Ph.D. thesis)

TWO-WEEK LOAN COPY

This is a Library Circulating Copy which may be borrowed for two weeks. For a personal retention copy, call Tech. Info. Division, Ext. 6782

June 1981

Donner Laboratory
Biology & Medicine Division

Prepared for the U.S. Department of Energy under Contract W-7405-ENG-48

LBL-11516

DISCLAIMER

This document was prepared as an account of work sponsored by the United States Government. While this document is believed to contain correct information, neither the United States Government nor any agency thereof, nor the Regents of the University of California, nor any of their employees, makes any warranty, express or implied, or assumes any legal responsibility for the accuracy, completeness, or usefulness of any information, apparatus, product, or process disclosed, or represents that its use would not infringe privately owned rights. Reference herein to any specific commercial product, process, or service by its trade name, trademark, manufacturer, or otherwise, does not necessarily constitute or imply its endorsement, recommendation, or favoring by the United States Government or any agency thereof, or the Regents of the University of California. The views and opinions of authors expressed herein do not necessarily state or reflect those of the United States Government or any agency thereof or the Regents of the University of California.

LBL 11516

FLUID DISTRIBUTION IN PROGRESSIVE PULMONARY EDEMA: A LOW TEMPERATURE SCANNING ELECTRON MICROSCOPY STUDY

Gregory Ross Hook

Ph.D. Thesis

Biophysics Department
Lawrence Berkeley Laboratory
University of California
Berkeley, CA 94720

This work was supported by the Director, Office of Energy Research, Office of Health and Environmental Research of the U.S. Department of Energy under Contract No. W-7405-ENG-48.

TABLE OF CONTENTS

FLUID DISTRIBUTION IN PROGRESSIVE PULMONARY EDEMA: A LOW TEMPERATURE SCANNING ELECTRON MICROSCOPY STUDY

ABSTRACT

High pressure pulmonary edema is a common medical disorder caused by venous hypertension following left ventricular heart failure. Abnormal fluid accumulation in the alveolar air spaces results in a life-threatening loss of respiratory function. The primary component of the fluid is water and therefore the study of water distribution in the alveolus can provide insight into high pressure pulmonary edema pathology.

However, the study of dimensional alterations in the alveolar microenvironment during pulmonary edema has been limited by the available methods of investigation. Light microscopy (LM) permits observation of large areas but does not resolve alveolar cell structure. Conventional thin section transmission electron microscopy (TEM) yields high resolution information, but sample preparatory techniques alter alveolar dimensions prior to observation. Further, section techniques obtain three dimensional information by statistical reconstruction and not by direct observation of the three dimensional alveolus. Freeze-fracture replica TEM provides indirect information on frozen hydrated lung, but replicas cannot preserve the convoluted surface of inflated alveoli over large areas of lung. Conventional scanning electron microscopy (SEM) permits high resolution, three dimensional observation, but conventional sample preparatory techniques also alter alveolar dimensions and remove water prior to observation.

The new method of freeze-fracture, low temperature SEM has been developed and applied to the study of pulmonary edema. This method combines freeze-fracture sample preservation with SEM observation and retains pulmonary fluids in the frozen hydrated state for direct three dimensional SEM imaging of alveoli. Quantitative measurements of alveolar structures resulting from high-pressure pulmonary edema were made from SEM micrographs.

Pathophysiological induction of high pressure pulmonary edema was achieved by fluid over-loading the vascular system of anesthetized dogs respirated at constant volume. Fluid loads of 0, 10, 30 and 50 percent body weight were studied in 4 dogs. Control and/or monitoring of blood pressure, airway pressures and blood analysis during the induction of edema coupled with in situ freeze fixation with liquid nitrogen allowed functional correlation with structural observation. The area of lung selected for SEM observation was 2 to 4.5 cm from bottom of the left lower lobe, and approximately 1 mm in from the diaphramatic plural surface to permit comparison of similar lung areas between dogs. Correlative assessment by low temperature LM examined the extent of edema formation in the interstitial spaces surrounding blood vessels and airways and wet to dry lung weight ratios were performed to determine the extent of gross pulmonary edema.

Alveolar fluid distribution resulting from induction of progressive high pressure pulmonary edema was determined by measuring cross fractured mid-alveolar wall width, alveolar corner area, alveolar width and alveolar depth from SEM stereopair micrographs. The average mid

ACKNOLWEDGEMENTS

I wish to thank the people who have contributed to this dissertation. Their professional ability is expert and their friendship is my most cherished memory.

Firstly, Dr. Thomas Hayes has skillfully guided the development and completion of this work. He generated academic excitement in a warm, personal atmosphere. The other members of the dessertation committee, Dr. John Schooley, Dr. Edward Lewis and Dr. Alex Nichols have consulted and reviewed the work.

Special thanks to Dr. Norman Staub of the U.C., San Francisco Cardiovascular Research Institute, who courageously allowed me the use of his laboratory and Dr. Robert Conhaim who did much of the careful pathophysiology presented here. Also, thanks to Ms. Elizabeth Schultz, Mr. Oscar Osario, and Mr. Mike Grady for the assistance in the pathophysiology.

In addition, thanks to my close associates Dr. Jacob Bastacky, Dr. James Pawley, Dr. Gregory Finch, Mr. Michael Sprague, Mr. Clifford Lai, and Ms. Dorothy Sprague for their emotional support and stimulating academic discussions over the years I worked with them. They made the daily work possible and enjoyable.

Ms. Caroline Schooley has taught me the art of freeze-fracture and an appreciation for biology. Dr. Allan Nelson has helped me avoid many problems in completing a dissertation.

Thanks also to Mr. Peter Dowling and Mr. Chris Goodman for their machine work and Ms. Diana Morris for her word processing of the manuscript.

alveolar wall width significantly increased ($P < .05$) from 3 μm to approximately 6 μm for all fluid loads. All fluid loads resulted in average mid alveolar wall widths which were not significantly different at the $P < .05$ level. The average alveolar corner area increased ($P < .05$) continuously with fluid loading which resulted in changing the polyhedrial shaped gas spaced in the control animal, to rounded polyhedrial shaped gas spaces in the moderate high pressure animal, to spherical shaped gas spaces in the high pressure animals. The average alveolar width was 91 μm for the control and 82 μm for all fluid loads. The average alveolar depth was 50 μm for control and to 46 μm for all fluid loads. All fluid loads resulted in a constant average alveolar gas space which supports the hypothesis that individual alveoli attain a critical gas space volume before alveolar flooding occurs. From these measurements a model for alveolar fluid distribution resulting from progressive high pressure edema was made.

Most importantly, I wish to thank my wife, Vivian, whose love has made this all worthwhile.

This paper was supported by a predoctoral fellowship from the Associated Western Universities which I appreciated very much. This work was supported by the Biology and Medicine Division of the U.S. Department of energy under Contract No. W-7405-ENG-48.

INTRODUCTION

Pulmonary edema is the pathologic state in which an abnormal amount of fluid accumulates in the lungs. Instead of viewing pulmonary edema as a static pathology, a more complete definition would show pulmonary edema as an imbalance in normal fluid homeostasis where the rate of fluid flow through the lung has changed. The net fluid flow through any organ was determined by Starling (1896) to equal the conductance across the microvascular barrier times the driving force (see Appendix A). This relationship has been used by Guyton and Lyndsey (1959) to classify pulmonary edema into two groups: edema due to changes in the conductance (permeability edema), and edema due to changes in the driving pressure (high pressure edema). The two forms can be differentiated on the basis of edema fluid composition, ultrastructural alterations and causative agent. Permeability edema results in edema fluid with high protein concentration (Vreim and Staub, 1976), structural damage to endothelial and epithelial cells and is commonly caused by inhalation of noxious gases (Plopper et al., 1973). High pressure edema results in edema fluid with low protein concentration (Vreim and Staub, 1976), little or no structural damage to endothelial or epithelial cells and commonly occurs in heart failure (Levine et al., 1967). Between these extremes are several categories where the etiology and pathology are more obscure. The subject of this study is the fluid distribution which results from high pressure pulmonary edema.

Fluid filling of the alveolar air space is the final, acute phase of pulmonary edema development. Said et al. (1964) showed that only

the alveolar flooding stage was pathophysiologically important in stopping gas exchange across the alveolus. Staub (1967) has emphasized that a fuller understanding of the edema process depends on events much earlier than alveolar flooding and has induced progressive high pressure edema with increasing vascular fluid loads in dogs in order to study the alveolar fluid distribution resulting from progressive edema.

The lung is a unique organ in having extracellular interstitial and extracellular alveolar gas compartments with each compartment having different fluid dynamics. In reviews by Simionescu (1975), Renkin (1977), and Staub (1980), the routes of fluid movement through the lung have been summarized. In normal lung, there is a continuous fluid and protein flow through the interstitial space. Fluid and protein leave the plasma, cross the microvascular endothelium, enter the interstitium and return via the lymphatics or by direct reabsorption into the plasma. Woolverton et al. (1978) showed the primary leakage site across the endothelium is in the vessels exposed to alveolar pressure which includes most of the alveolar wall capillaries and some small arterioles and venules. Possible routes across the endothelial barrier are through intercellular endothelial juntions, membrane pores or vessicles, large non selective leaks and across the cell membranes in the case of permeable molecules. In contrast, the alveolar epithelium is very impermeable to all hydrophilic solutes and there is no passive flux across it. Althrough the site of fluid leakage into the alveolar air space is not known, Staub (1980) postulates that the terminal airway epithelium may normally be conductive to fluids. According to this

hypothesis, high pressure pulmonary edema could cause overlfow of fluids through the terminal airways and retrograde flow into the alveoli.

A central problem in pulmonary edema research is the difficulty in obtaining quantitative data, especially in the early stages of edema development. This was appreciated early on by Visscher et al. (1956) when they wrote "The quantification of the edema state is a difficult probem at any site. It is particularly so in the lung because the organ is relatively inaccessible and because standards of reference are difficult to establish." Rusznyak et al. (1967) wrote that histologic examination was the most sensitive way to quantify edema but it was not until Staub et al. (1967) utilized light microscopy (LM) of frozen fixed lungs from dogs in which pulmonary edema was induced under controlled pathophysiological conditions that the sequence of fluid accumulation during pulmonary edema was ellucidated. These researchers studied high-pressure and permeability edema and concluded that although the primary mechanisms for edema formation were different, both types of edema showed the same histological sequence of fluid accumulation in the various compartments of the lung. They determined that fluid first appeared in the loose interstitial connective tissue compartment around the conducting vessels and airways to form the perivascular "fluid cuffs." This was followed by alveolar wall thickening and finally by acute alveolar flooding after the interstitial compartment was well filled. Alveolar flooding is rapid and independent and the total volume of the alveolar space (gas plus fluid) of each

fluid-filled alveolus was reduced. Iliff (1971) showed that lung weight need only increase by 4-6 percent before histological evidence of perivascular fluid cuffing appeared. Gee and Williams (1979) quantitated the fluid distribution in frozen edematous dog lung by light microscopic statistical reconstruction of perivascular fluid cuffs and determined the cuffs have a substantial volume that approached as a maximum the total extravascular water volume of normal lungs. LM examination, if conducted on frozen fixed lungs and utilizing randomized sampling procedures, offers quantitative measurement of pulmonary edema that is very valuable in studying the early accumulation of extravascular water where most other methods of investigation are insensitive.

However, LM investigation is limited in resolution by the wavelength of light and in the depth of focus to a thin plane through the sample. The resolution limit of LM did not allow the cellular structure of the alveolar wall to be resolved and it was not until development of thin section technique and examination in the electron microscope that the alveolar cellular structure was determined. In addition, sectioning the sample required that three dimensional information be determined by statistical reconstruction of an average structure and not by direct observation of individual alveoli. These limitations restricted the information that could be obtained by this method with respect to the fluid accumulation in the small, three dimensional alveolar walls and spaces.

Transmission electron microscopy (TEM) of their sections, on the other hand, has provided high resolution information on the ultrastructure of the alveolus. Cotrell et al. (1967) and Ryan (1969) described the eccentric placement of the capillaries in the alveolar wall in relation to the air spaces and connective tissue. Gehr and Weibel (1974) and Gehr et al. (1978) showed the alveolar septa was lined on both sides by a continuous epithelium and that most of the surface was composed of thin squamous type I epithelial cells with type II and type III cells interspersed into the surface cell lining. The capillary vasculature was bounded without interruption by a layer of endothelial cells which were continuous with the pulmonary arteries and veins. In the alveolar septa, one side of the capillary was usually close to one of the epithelial surfaces. In this region, both the alveolar epithelium and endothelium were attenuated and the basement membranes fused so that the air to blood gas diffusion distance was < 1 μm. This was defined as the "thin" portion of the air-blood barrier. On the other side of the capillary, between the epithelial cell layer, was the interstitial space that formed the "thick" side of the septal wall. Weibel and Gil (1968) and Gil and Weibel (1970) showed the epithelium was covered with an extracellular fluid, the surfactant, which formed the interface with the air and which pooled in the depressions and corners of the alveolar surface.

Ultrastructural changes associated with high-pressure pulmonary edema were studied using TEM thin section techiques. Fishman (1972) showed alveolar wall interstitial edema preferentially accumulated on

the "thick" side of the alveolar septum. Schneeberger-Keeley and Karnofsky (1968), Pietra et al. (1973), and Schneeberger (1978), experimented under conditions of normal and high-pressure pulmonary edema and studied the distribution of macromolecular tracers in thin section TEM. They found that macromolecular tracers were confined to the vasculature lumens under normal pressure but when the pulmonary pressure was increased to 3 times normal (65 cm H_2O), interendothelial vascular cell junctions appeared to open and tracers were found in the interstitial space but not in the alveolar air space. Further increases in pulmonary pressure resulted in alveolar flooding but epithelial cells and epithelial cell junctions remained intact. These experiments indicated pores of the intercellular endothelial junctions could stretch open and permit fluid flow into the interstitium during high pressure pulmonary edema and the epithelial cell lining posed a formidable barrier to fluid flow into the alveolar space.

De Fouw and Berendsen (1978) and De Fouw (1980) applied statistical morphometric reconstruction analysis to TEM thin section micrographs of high pressure induced edematous dog lung. Edematous lungs, fixed by airway perfusion or vascular perfusion of chemical fixatives, shoed an increased width in the alveolar septem from control lungs. The increased se]tum width was due to an increase n the interstitial compartment of the alveolar se]tem and the endothelial and epithelial cellular compartments were unchanged in thickness. More pinocytotic vesicles were found in both endothelial and type I epithelial cells in edematous lungs from which these researchs concluded that transendothelial and transeptithelial vesicular transport may contribute to fluid flow in pulmonary edema.

Although a great deal has been learned by thin section TEM investigation, the required chemical fixation, dehydration and embedment introduces artifacts which limit the information that can be obtained. Defouw (1980) pointed out that chemical fixation procedures may not adequately preserve alveolar dimensions for quantitative assessment of changes in alveolar sizes after edema production. Mazzoni et al. (1980) have shown fixation, dehydration and embeddment prior to observation alters lung structure by causing shrinkage. The removal of water during sample preparation made it impossible to observe fluid distribution directly by conventional TEM thin section techniques. Further, thin section work allowed observation of very limited sections through alveoli. Three dimensional information on alveolar structure could only be determined by statistical reconstruction on an average alveolus with interconnections between alveoli and other lung structures difficult to determine.

Moore and Meuhentaler (1963) developed freeze-fracture TEM replica techniques to give indirect information on biological structures preserved in the frozen state. Branton (1966) has shown this technique reveals the internal structure of biological membranes and especially of intramembrane protein aggregates in the plane of the membrane. The process is to freeze rapidly small, chemically fixed or unfixed (Hauser, 1979) samples, freeze fracture in a low temperature, high vacuum environment and then evaporatively coat the freshly exposed surface with a layer of carbon platinum (C-Pt). A replica of the surface is then made by digestion of all cellular material leaving the

fragile C-Pt foil replica of the surface for SEM observation. The freeze-fracture studies by Inone et al. (1976) on fluid filled edematous dog lung have shown the interendothelial cell junctions become disrupted while the interepithelial cell junctions preserve a tight seal during high pressure pulmonary edema. Untersee et al. (1971) using freeze fracture TEM replica techniques showed the hypophase of the epithelial surface lining film formed a continuous but inhomogeneous layer on the alveolar surface.

While an excellent tool for indirect morphological studies of frozen-hydrated material, freeze-fracture TEM replica studies present two major problems which limit the information obtained on pulmonary edema development. First, the need to use small samples usually results in the removal of a small portion of the lung for freezing. This poses a unique problem in studying the lung because alveolar structure depends on airway inflation pressure which can only be assured in an intact whole lung lobe. Second, the replica is very delicate and large areas of the convoluted alveolar surface cannot be preserved in replica form. Upon digestion, the replica breaks into small fragments because the deep topographical features in the alveolus do not permit a complete, strong film to be deposited over the entire surface. Therefore, replica of air inflated lungs do not allow large areas to be examined and makes interpretation of connections between structures difficult.

Three dimensional topographical qualitative information on large areas of lung has been obtained by Nowell and Tyler (1971) using the

scanning electron microscope (SEM) in the secondary electron emission mode. The high magnification and great depth of focus in this system allows observation of the alveolar surface and connections with surrounding structures. Using SEM, the fibrous structure of the alveolar septum was shown by Wang and Ying (1977) to consist of a flat network of fine connective tissue fibers interlaced with the capillary network. Gil et al. (1979) utilized SEM to study the surface texture of lungs inflated with either air or saline at different inflation volumes and fixed by vascular perfusion. Air filled lungs were found to have smooth surface except at low lung volumes while saline filled lungs had irregular surfaces due to undulating walls and bulging capillaries at all lung volumes. In air filled lungs, pleating and folding of the alveolar septa was observed while saline-filled lungs did not exhibit pleats. Parra et al. (1978) and Takaro (1979) used SEM and TEM to study the ultrastructure of canine interalveolar pores of Kohn prepared by airway and vascular fixation. They determined airway perfusion of chemical fixative removed the surfactant surface lining material to reveal an average of 19 alveolar pores (3 μm in diameter) in each alveolus. Vascular perfusion of fixative preserved the surfactant lining and three pores per alveolus were observed. They concluded the alveolar while pores of normal dogs were bridged by and filled with lung surfactant. Schafer et al. (1975) studied surface morphology of neurologically induced pulmonary edema and observed capillary congestion, intraalveolar proteinous exudate and capillary hemorrhage.

However, conventional SEM sample preparatory techniques employed by these researchers required chemical fixation, dehydration and drying

prior to SEM observation. Boyde et al., 1977 and Boyde, 1978, has shown these procedures can cause soft biological samples to shrink up to 30 percent in linear dimension; furthermore, the shrinkage may not be isotropic. This methodology therefore can introduce a large error in sample dimensions and eliminates direct observation of the fluid distribution.

An alternative method of SEM sample preservation has been the development of low temperature SEM (Franks, 1977; Fujikawa and Nei (1978), Echlin, (1978) and Pawley et al. (1980)). This method offers several advantages over conventional SEM preparatory techniques that are important in the study of pulmonary edema; in particular, low temperature SEM preserves the sample in the frozen-hydrated state, minimizes fluid redistribution (Echlin, 1978) and minimizes sample shrinkage (Boyde, 1978). Early qualitative attempts at low temperature SEM observation of frozen-hyhdrated lung by Groniowski and Walski (1974) were limited by atmospheric water condensation on the cold sample surface during the transfer of the frozen sample through the air into the SEM. These researchers had no cold stage to maintain the lung in frozen state and, therefore, the lung could not be observed very long before warming up.

The development of a low-temperature sample preparation chamber attached to a SEM and a cold stage equipped with a Joule-Thompson refrigerator (Pawley and Norton, 1978) combined freeze fracture sample preparation in a low temperature, high vacuum environment with SEM observation of the frozen-hydrated surface. Without breaking vacuum,

in vacuo transfer of the sample from the cryo preparation chamber to the SEM permitted observation of a clean fractured surface (Pawley et al., 1978). Fractured biological surfaces prepared in this system were shown by Hook and Schooley (1978) and Pawley et al. (1980) to exhibit characteristic structures observed by correlative TEM freeze-fracture replica techniques. Although the resolution limit was approximately 30 nm and did not permit direct observation of intermembrane particles, replicas of fractured surfaces made in this system exhibited intermembrane particles when the conductive Pt-C SEM coating was observed as a replica in the TEM (Hook and Schooley, 1978). Earlier work of Hook et al., (1980), established the methodology for handling from lung samples for freeze-fracture SEM observation of cross fractured alveolar septa and alveolar surfaces. It seemed, therefore, that low temperature SEM was an appropriate tool to observe alveolar structures during progressive pulmonary edema.

Hayes (1980) has discussed the importance of stereo observation of SEM samples in order to obtain information on three dimensional structure from two dimensional micrographs. Quantitation of SEM micrographs has been discussed by Boyde (1970), Boyde (1973), Howell (1978), and Howell (1980). Therefore, stereopair micrographs were taken and presented here in stereo form. A principle error in quantitation of soft biological samples in conventional SEM was sample shrinkage during preparation. However, observation of frozen-hydrated material minimized sample shrinkage and, therefore, permitted more accurate quantitation of sample sizes. Other errors in stereo SEM photogrammetry are well understood (Howell, 1978) and can be minimized by SEM calibration and correct SEM operation.

METHODS

I. Pathophysiological Induction of High Pressure Pulmonary Edema

Small mongrel dogs (10-18 kg of both sexes) were anesthetized by intravenous injection of sodium diabutal to effect, placed on their backs on a surgical table, and the fur shaved from the neck, chest, and left rear thigh in prearation for surgery. A Bovie Model 400 (Sybron Medical Products, Rochester, N.Y.) electric arc and forceps were used to expose the trachea, a treachonomy performed, and the trachea tube connected to a Harvard respirator (type 607; Harvard Instruments, Millis, Mass.) to provide an air inspiratory pressure of 10 cm H_2O at a constant volume and a rate of 12 breaths/minute. A "T" connector in the respiration line was attached by a plastic tube to an O_2 gas pressure regulator and this tube was clamped closed. This respiratory system allowed rapid conversion from cyclic air respiration to continuous O_2 pressure respiration at the moment of freezing. A needle inserted into the plastic trachea tube was connected to a Statheim strain gauge pressure transducer for monitoring airway (A) pressure (all pressures monitored with Models 131TC, P23AC, P236b, Hato-Rey, Puerto Rico).

Pulmonary artery (PA) pressure was monitored by insertion of a Schwan-Ganz catheter Model 5F (Edwards Laboratories, Santa Ana, CA) through the exposed right exterior jugular vein, the right atrium, the right ventricle into the pulmonary artery and connecting to a strain gauge pressure transducer. Left ventricle end diasstolic (LVED) pressure was monitored by another catheter inserted via the exposed

right common carotid artery, the aortic artery into the left ventricle and connected to a strain gauge pressure transducer.

The femoral artery and vein was surgically exposed on the left thigh and a catheter was inserted into the femoral artery and connected to a strain gauge pressure transducer for measurement of femoral arterial pressure (FA). This catheter was also used to withdraw arterial blood samples for blood analysis. A venous catheter was placed in the femoral vein for administration of fluid to induce high pressure pulmonary edema. This catheter was also used to give more anesthesia should the dog show signs of awakening. Special care was taken to maintain the animal in deep anesthesia throughout the experiment. Figure 1 shows an experimental animal with all catheters and respiratory tubes in place.

The outputs from the pressure transducers were amplified and recorded continuously during the entire experiment on a multichannel amplifier-recorder polygraph Model 7 (Grass Instruments, Quincy, Mass.) shown in Figure 2. The pressure transducers were positioned at the right of the animal's heart, 10 cm above the table, and each pressure transducer and amplifier channel was calibrated before each experiment with a water or mercury manometer.

After the trachea tube and all catheters are positioned, 30 minutes was timed to establish a physiological baseline and the first blood sample was taken for blood gas analysis, protein content and hematocrit. Normal saline was then loaded into all experimental animals at a rate of 1 percent body weight/minute by suspending the fluid approximately 90 cm above the dog as seen in Figure 3. Experimental fluid

loads of 10, 30 and 50 percent body weight were studied. This procedure insured that all animals received a fluid load at a constant rate but the total volume and length of time for loading varied with experimental fluid loads. Fluid loading would stop when the desired percent body weight of fluid was loaded or gross pulmonary edema developed.

After fluid loading, 30 minutes was timed to achieve a return to physiological steady state. At the end of this time pressures returned to initial values and a second arterial blood sample was taken to determine blood gases, hematocrit, hemoglobin, protein content and wet/dry ratio. The chest was then opened by mid sternum incision and lateral cutting of the ribs at the diaphram taking care not to damage the lungs. Simultaneously upon opening the chest, an end expiratory pressure of 5 cm H_2O was added to the cyclic respiration to prevent the lungs from totally collapsing upon expiration. The lungs were exposed by tieing back the cut rib cage and cyclic respiration was clamped off and the continuous pressure O_2 supply used for inflation. The lungs were inflated to 30 cm H_2O and deflated to 5 cm H_2O three times by manually clamping the plastic exhaust tube from the continuous pressure supply. On the third inflation, the lungs are deflated to 20 cm H_2O and two parallel lines are rapidly painted with toluidine blue on the diaphramatic plural surface of both right and left lower lobes. The lower line was marked approximately 2.5 cm from the bottom of the lung and the second line was 2 cm above the first line as shown in Figure 4. The zone between the lines defined the area investigated by low temperature light and scanning electron microscopy. Opening the chest took approximately 15 to 20 minutes and the lungs were exposed to O_2 for 5 minutes.

The O_2 inflated, marked lungs were then frozen in situ by rapidly pouring several liters of liquid nitrogen over the diaphramatic surface of the lung to fix all pulmonary fluids in the frozen state as seen in Figures 5 and 6. Freezing the two lobes took approximately five minutes but the diaphramatic surface of the lung froze in less than a half minute. The A, PA, LVED, and FA pressures were recorded during the freeze fixation. The airway pressure fluctuated during freezing but averaged 20 cm H_2O while the pulmonary artery pressure rose rapidly as the lung froze. The frozen lungs were removed from the body and stored in liquid nitrogen.

II. LOW TEMPERATURE LIGHT MICROSCOPY

The frozen right lower lobe was used for light microscopic observation of fluid distribution. A sample from between the marking lines was cut from the lobe in a -30°C Harris cryostat (North Bullerich, Mass.) and mounted to a cooled holder with low temperature glue. The block surface was cut flat with a Riechert microtome at -30°C in the cryostat. The cut, frozen block was enclosed in a metal bottom container with a Petri plate cover, removed from the cryostat and placed on a metal stage pre-cooled by a dry ice ethanol slush. The surface of the frozen block was photographed at 5x magnification using a Nicon 35 mm camera equipped with bellows extension and microlens. Photographs were taken on Kodachrome 64 slide film using two strobe lights for illumination. Low temperature light microscopy was useful for determining the extent of pervascular cuffing, alveolar flooding and uniformity of sample inflation.

III. WET/DRY LUNG WEIGHT RATIO DETERMINATION

Analytical Procedures

Wet/dry lung weight ratios were determined by the method of Pearce et al. (1965)as modified by Selinger et al. (1975) on the right lower lobe on the lung remaining after low temperature LM. The frozen lung was thawed in a covered container, weighed and homogenized with equal volume of distilled water in a large blender (Model 5011, Waring Prod., New Harford, Conn.) Two 15 ml Corex (Dupont-Sorvall, Newton, Conn.) tubes were filled with well stirred lung homogenate and centrifuged at 30,000 g (DuPont-Sorvall, RC 2-b) at 5°C to obtain a clear red supernatant. Lung homogenate, lung supernatant, whole blood and plasma was used as necessary to determine the hematocrit, hemoglobin concentration, total proteins and water content. Hemoglobin in the whole blood and the clear lung supernatant was measured using the cyanmetremoglobin method and total protein by the Biuvet method from Henry (1964). Water content of lung hemogenate, supernatant and whole blood was determined from duplicate weighed samples dried at 85°C for 96 hours.

Calculations for Wet/Dry Lung Weight Ratio

The calculations used to determine wet/dry weight ratio were based on repeated application of the conservation of matter principle as described by Selinger et al. (1975). These calculations estimate residual blood content of the lungs in order to determine the extravascular water concentration of the lung itself. The equations and a brief description of the nomenclature used follows:

Blood content: The blood content of the lung, Q_b, was calculated from the equation:

$$Q_b = Q_h \times \frac{(Hb)s}{(Hb)b} \times \frac{Fwh}{Fws} \times \frac{(D)b}{(D)s} \quad (1)$$

where Qh = weight of lung hemogenate; (Hb)s and (Hb)b were the hemoglobin concentrations in the lung supernatant (s) and whole blood (b), respectively, Fwh and Fws were the fractional water contents of the lung homogenate and lung supernate, respectively; D_b and D_s were the densities of the blood and supernate, whose quotent equals a constant of 1.03 for dog as determined by Staub (personal communication).

Extravascular lung water: The total extravascular water content, QwL, and the dry weight of the lung, dQL, were calculated by the following equations

$$QwL = (Qh \times Fwh) - (Q_b \times Fwb) - Qw + \quad (2)$$

$$dQL = QLb - Qb - Qwl \quad (3)$$

where QLB = weight of wet lung; Fwb = fractional water content of blood; Qw^+ = amount of water added to the lung during homogenization.

The wet/dry lung weight ratio after correcting for the blood volume is then QWL/dQL.

IV. LOW TEMPERATURE SEM SAMPLE PREPARATION

The frozen left lower lobe was used for SEM observation. Under LN_2, the frozen segment was cut along the marking lines using a cooled hack saw blade and then cut parallel to the disphramatic pleural surface 1 cm into the lung. From this segment a .5 cm diameter by 1 cm long lung cylinder was made by orthogonally core boring the segment at

the diapharamtic pleural surface with a precooled punch under LN_2 (see Figure 8). The frozen lung cylinder (see Figure 9) was mounted pleural surface down, onto a precooled SEM sample stub with a sliding clamp mechanical holder (see Figure 10).

The stub and sample was rapidly transferred (<1 minute) in a LN_2 cooled brass cold shroud via an airlock to the high vacuum, low temperature environment of an AMR Biochamber (Pawley and Norton, 1978), as seen in Figure 11. The Biochamber sample separation chamber is attached directly to an AMR 1000A SEM and permitted freeze-fracture and coating while maintaining the lung at low temperature in the frozen-hydrated state. The sample shuttle temperature was monitored throughout the system. The sample was fractured at a temperature < -160°C, in a vacuum of 1×10^{-5} torr. The fractured surface was evaporatively coated with a gold (Au) layer 14 nm thick while tilting and rotating (Hook et al., 1980). The sample was transferred in vacuo to the low temperature SEM stage for examination in the frozen hydrated state (see Figure 12).

V. LOW TEMPERATURE SEM SYSTEM CALIBRATION

The freeze-fractured sample was maintained at a temperature below -140°C during SEM observation by the Joule Thompson, high pressure (1200 p.s.i.) nitrogen gas refrigerator mounted in the microscope stage. Sample contamination and radient heat transfer was minimized during observation by a -160°C copper cryoshield above the sample.

Consistant SEM operating conditions were used during examination of samples. For Au coated samples, the electron beam had an

accelerating voltage of 10 kv, a specimen current of 5×10^{-12} amps and was corrected for astigmation. For uncoated samples, the electron beam had an accelerating voltage of 5 Kv and a specimen current of 6×10^{-12} amps and was corrected for astigmation. With the magnification zoom control in the calibrated position, a beam working distance of 12 mm was set by ringing the course final lens (focus) current. Ringing the final lens minimized variation in magnification due to hysterisis in the electric/magnetic field of the final lens between observations and positions the focal point of the beam at the calibrated magnification position. Once this position was achieved, the final lens current was not changed during observation. The sample was brought into focus by raising or lowering the sample with the z stage control to insure constant magnification without beam rotation between successive micrographs. Stepwise changes in magnification were made using the fixed stop magnification switch and each magnification step was checked periodically with a standard wire mesh grid (No. 31700, Ladd Industries, Burlington, Vermont). The console power to the microscope remained on between successive days of operation to minimize variation in magnification.

Stereo pair micrographs were taken to permit measurement of alveolar structures. Stereo pairs were taken around the y axis of tilt with a 9° tilt difference between stereo pair micrographs. The same tilt stage settings were approached in the same way for all micrographs to minimize tilt errors due to mechanical stage lash.

The tilt difference between stereopairs was calibrated at room temperature on the Mark II cold stage removed from the microscope. A

circular compass with a vernier setting and 2x magnification eye piece was attached to the stage on the axis of tilt and allowed observation of changes in tilt. Repetitively tilting the stage to the same two tilt settings while noting the direction of approach showed the change in tilt at the two settings to be 9°(±0.1°) at room temperature. No attempt was made to calibrate the stage at low temperature.

VI. LOW TEMPERATURE SEM SAMPLING PROCEDURE

A random sampling procedure was done on the fractured surface of each frozen-hydrated lung. The sample was centered in the display cathode ray tube (CRT) at a magnification of 20 x and stereo micrographs taken of the fracture surface. Two random numbers were selected from a random number table to determine the amount of travel for the x and y' stage controls and the clockwise/counter-clockwise direction of rotation was determined by the even/odd nature of the last digit from the random number. At this random position, the magnification was increased to 500x and an area selected for stereophotography if the following criteria are met:

a) The area contained a cross-fractured alveolar septa normal to the aspect of the electron beam.

b) The area has not been previously recorded.

c) The area is not grossly damaged.

VII. LOW TEMPERATURE SEM MEASUREMENT OF ALVEOLAR DIMENSIONS

All measurements were made with a simple stereometer (Wild, Model ST4, Heerbrug, Switzerland) to visualize the three dimensional shape of the alveolar surface. Occulars on the stereometer magnified the alveolar structures to 1500x and the measurement rules to 3x (see Figure 13).

Conversion of measured dimensions (D_x, D_y, D_z) to real dimensions (d_x, d_y, d_z) were made using parallel plane projection formulae;

$$D_x = Md_x$$

$$D_y = Md_y$$

and $$D_z = P/M2\sin(\phi/2)$$

where: M = magnification of the micrograph (500x)

P = parallax measurement (mm)

ϕ = the difference in tilt angle between stereopairs (9°).

A. Measurement of Cross Fractured Alveolar Wall Width

Measurements were made on cross fractured walls at midpoint between alveolar corners. Only cross fractures normal to the viewing aspect and orthogonal to the alveolar surface were selected for measurement. Measurements were made in the x,y plane using a .1 mm reticle.

B. Measurement of Cross Fractured Alveolar Corner Area.

Two measurements were made of each junction formed between three cross fractured alveolar walls. The first measurement, b, was made between two points at the maximum radius of curvature on two adjacent cross fractured alveolar walls. The second measurement, h, was made between the midpoint of measurement b and the maximum radius of curvature on the third cross fractured alveolar wall. The cross fractured alveolar corner area was then approximated by the triangular area, A, calculated from:

$$A = 1/2\ bh$$

C. Measurement of Alveolar Cross Fracture Depth (z)

The alveolar cross fracture depth was determined from parallax measurements made with a parallax bar (Gordon Enterprises, Model 1226E). The parallax was measured from the deepest point in an alveolus to the highest cross fractured wall.

D. Measurement of Alveolar Cross Fracture Widths

The two points used to determine the cross fractured alveolar depth were used to define a line across the fractured alveolus. The length of this line from inside edge to inside edge of the fractured wall, was defined as the alveolar cross fracture width.

VIII. STATISTICAL ANALYSIS OF ALVEOLAR DIMENSIONS

Table 1 lists the number of measurements made in this study. After the cross fractured wall width, corner area, alveolar width and alveolar depth measurements were made, statistical analysis of the data was performed. An arithmetic average, variance, standard deviation, standard error, frequency distribution and hypothesis testing of the difference between means using the Bonferoni Modified Student's t test were calculated and/or graphed for each structure. See Appendix B for equations used in the statistical calculations.

TABLE 1

LOW TEMPERATURE SEM SAMPLING

Group: Body Wt. Fluid load	Dogs	Number of: Lung Cylinders	Alveolar Areas (500X)	Alveolar Measurements			
				Wall Width	depth Area	corner Width	
0	1	11	46	77	76	66	97
10	1	10	40	47	47	53	98
30	1	11	47	96	96	73	153
50	1	9	35	48	48	46	91

RESULTS

I. Pathophysiological Data

Pulmonary artery pressure, left ventricular end diastolic pressure, airway pressure and systemic pressure were continuously monitored during fluid loading. Analysis of the polygraph pressure data showed the average pulmomary artery pressure, left ventricular end diastolic pressure and inspiratory airway pressure increased in a smooth, continuous fashion during fluid loadings, reached a maximum at the end of the fluid loading, and returned to normal levels in a smooth, continuous manner 30 minutes after fluid loading was completed. Systemic blood pressure did not change during or after fluid loading. Figure 14 shows these pressures 30 min before, at the end, and 30 min after fluid loading. Pulmonary artery pressure (P_{PA}) increased 3 fold from baseline at the end of 10 percent body weight fluid load and 7 fold from baseline at the end of 30 percent and 50 percent body weight fluid loads. Left ventricular end diastolic (P_{LVED})pressure increased 3 fold at the end of 10 percent body weight fluid load and 7 fold at the end of 30 percent and 50 percent fluid loads. The P_{PA} and P_{LVED} pressures are significant because they determine the pulmonary hydrodynamic pressure. The hemodynamic force generating high pressure pulmonary edema is the net sum of the pulmonary hydrodynamic and osmotic pressures. Inspiratory airway pressure increased slightly from normal at the end of 10 percent body weight fluid load, 2.5 fold from normal in the 30 percent body weight fluid load and 4 fold from normal in the 50 percent body weight fluid load. The increase in airway

pressure during fluid loading was because vascular congestion caused pulmonary stiffening (Hogg et al.). The respiratory pressure is important because it keeps the alveoli open. The systemic arterial pressure did not change with fluid loading.

Arterial blood samples were taken before and after fluid loading; Figure 15 shows the results of blood gas analysis. The pH decrease resulting from 30 percent and 50 percent body weight fluid loads was probably due to the non-buffered pH 7.0 normal saline used to infuse the dogs. The decrease in PO_2 with higher fluid loads probably reflects the decreased efficiency in O_2 uptake due to pulmonary edema although the lower levels were adequate to sustain life in the dogs. The decreased efficiency of PO_2 uptake was probably due to a decrease in the number of open alveoli and pulmonary vascular redistribution. The blood hematocrit before and after fluid loading shows that the hematocrit decreases after loading probably reflecting an increase in blood fluid volume due to the infused fluid load. Total blood protein concentration decreased with fluid loading which caused a decrease in vascular osmotic pressure. The decrease in osmotic pressure decreases the amount of water retained in the vascular system and can be quite significant because 1 mosmole = 19 cm H_2O. PCO_2 and HCO_3^- levels did not appreciately change after fluid loading.

<u>In situ</u> freeze fixation was used to preserve lung structure with pulmonary fluids in place. Correlation of lung structure with physiological pressures was achieved because pressures could be monitored and controlled at the time of freeze fixation. Figure 7 shows as an

example the strip chart recording obtained from the dog at the moment of lung freeze fixation. Thus, this technique can yield information on physiologically important pressures which can influence lung structure at the moment of fixation.

Table 2 shows the calculated wet/dry weight ratios for each animal. The control and ten percent fluid load had the same wet/dry ratio while the thirty and fifty percent fluid load had a marked increase in the wet/dry ratios.

TABLE 2

WET/DRY LUNG WEIGHT RATIOS (EXCLUDING BLOOD WEIGHT)

Fluid Load	Ratio
Control	4.5
10	4.5
30	7.0
50	14.1

See text for discussion of values.

II. Low Temperature Light Micrograph Data

A light micrograph of normal frozen lung is shown at magnification 20X in Figure 16. The cut airway and blood vessels have thin walls with no evidence of fluid accumulation in the surrounding perivascular space. Figure 17 is a light micrograph at 20X of frozen lung from the 10 percent body weight fluid loaded dog. Airways and blood vessels have thicker walls than normal which is evidence of fluid accumulation in the surrounding perivascular space. Figure 18 is a light micrograph

at 20X of the frozen lung from the 30 percent body weight fluid loaded dog. The thick walls surrounding the airways and blood vessels shows that a large amount of fluid has accumulated in the surrounding perivascular space. Figure 19 is a light micrograph at 20X of frozen lung from a 50 percent body weight fluid loaded dog and shows the extensive engorgement of the perivascular space surrounding the blood vessels. These micrographs document that the experimental fluid loaded lungs developed characteristic perivascular fluid cuffs surrounding the airways and blood vessels.

III. Low Temperature SEM Stereomicrograph data

Figure 20 shows a stereopair, low temperature SEM micrograph of freeze-fractured, Au coated, control dog lung at a magnification of 20X. (To observe stereo effect, see Appendix C for instructions on use of stereo glasses.) The lung is seen to have a convoluted topography and many alveolar surfaces were exposed by cross-fracturing the alveolar walls. The thin alveolar walls define polyhedral shaped airspaces. The outlined box shows the location of the next stereopair micrograph. Figure 21 shows this area at 500X to reveal alveolar surfaces and crossfractured alveolar walls. Thin walls (3 μ) have been cross fractured and junctions between three alveolar walls are seen in crossfracture as small triangular areas. The polyhedrial shape of the airspace defined by the walls is apparent. The alveolar surface has an inhomogeneous texture with cubic structures decorating the surface. These cubic forms are probably due to ice crystal contamination because observation of the freeze drying process shows these structures sublime

upon warming uncoated samples. The outlined area locates the area shown next in Figure 22. This area has been photographically enlarged 3X making the print magnification 1500X to show the alveolar corner area and wall as it was observed and measured in the stereometer equipped with 3X occulars.

Figure 23 is a 20X magnification stereopair micrograph of freeze-fractured, Au coated, 10 percent body weight fluid loaded, dog lung. Again, a convoluted topography is seen with exposure of many cross fractured alveoli and the walls appear slightly thicker. The thickness is better appreciated at the 500X magnification micrograph in Figure 24 which shows the alveolar walls of the 10 percent fluid loaded dog have an average uniform thickness. The wall appears wider than in the control lung and defines a polyhedral shaped air space with rounded corners. The aveolar cross-fractured corner area is larger in the 10 percent fluid loaded dog lung than in the control lung. A prominent feature of the 10 percent fluid loaded alveolus is the irregular surface area exhibiting a networks of lumps. These lumps are presumably the result of fluid distending the alveolar surface above areas in the capillary network because they have a characteristic capillary morphology. This distended capillary network structure was only occassionally observed in the control lung, frequently seen in 10 percent body weight fluid loaded lung and never seen in the 30 percent or 50 percent body weight fluid loaded lungs. Figure 25 shows the alveolar walls and corner area at high magnification 1500X.

Figure 26 is the 20X magnification stereopair image of the cross-fractured, Au coated, 30 percent fluid loaded dog lung. Again numerous alveoli are revealed by cross-fracture but appear to have rounded air-spaces. Figure 26 is a higher magnification of the outlined area and shows the rounded shape of the airspace of the 30 percent fluid loaded lung and increased cross-fractured corner area and wall width. The average alveolar wall width does not appear as uniform in the 30 percent fluid loaded lung as in the control lung with some walls being thick and others thin. A thick wall is outlined and shown photographically enlarged 3X in Figure 28. The cross-fractured wall has a rough and smooth texture with the rough surface due to fracturing through cellular structures and the smooth area a result of fracturing fluid filled areas.

Figure 29 shows the fractured, Au coated surface of the 50 percent body weight fluid loaded dog lung at 20X; note the rounded airspaces. Figure 30 at 500X shows the mid alveolar wall width appears thicker and the cross-fractured corner area larger in the 50 percent fluid loaded dog than in the control dog. The outlined area shows the locations of Figure 31 photographically enlarged 3X. The cross-fractured walls are shown after the sublimation of water from the fractured surface to reveal the non-volitile components embedded in the wall. Freeze-etching is useful for distinguishing cellular components from fluid filled spaces. The alveolar surface was also subjected to freeze etching but the surface appears smooth and continuous which indicates the alveolar surface of the edematous lung has a non-volitile component lining the surface (probably surfactant).

Figure 32 is of an uncoated frozen-hydrated lung dog lung photographed at -160°C and shows two flat membranous structures. These structures were seen in all dog lungs prepared for low temperature examination and were formed spanning the width of alveoli or in the corners of alveoli. These structures are not cellular because freeze-drying the sample causes their collapse as seen in Figure 33 of the same area as in Figure 32 but at a temperature of -30°C. This documents that these structures depend on hydration for preservation and observation.

Figure 34 shows the alveolar surface of a control dog preserved by airway chemical fixation, dehydration and critical point drying. This method of preparation removed all alveolar surface lining material and reveals the epithelial cell surface structure and interalveolar pores of Kohn. The alveoli appear buckled which is probably due to the sample shrinkage during preparation. Contrasting this image with that obtained by low temperature SEM of frozen-hydrated normal lung shows how much the sample preparation effects the observed alveolar structure.

IV. LOW TEMPERATURE SEM MEASUREMENT DATA

Figure 35 is a graph of the mid-alveolar wall width measurements mean and standard error of the mean for increasing fluid loads. Figure 36 is a frequency distribution of mid alveolar wall widths for each fluid load. The Bonferoni Modified Student's t test for differences between the means of control and fluid loaded dogs showed all fluid loaded dogs had a significant ($P < .05$) increase in mid

alveolar wall width from control. The test showed no significant difference ($P > .05$) for width measurements between the means of fluid loaded dogs. Frequency distribution and standard error of the mean showed a normal distribution of measurements for control and 10 percent body weight fluid loaded dogs but a dispersed distribution of measurements for 30 percent and 50 percent body weight fluid loaded dogs. Thus, fluid loading resulted in a two fold increase in the mean mid alveolar wall width. Control and 10 percent fluid loaded mid alveolar wall width measurements approximated a Gaussian distribution while 30 and 50 percent fluid load measurements had a dispersed distribution.

The mid alveolar wall thickness was measured from the same data set at two different times. The student's t test for differences between means showed no significant ($P > .05$) difference between the means of the two measurements within each fluid load group. Therefore, it was concluded that measurement of the data was reproducible.

Figure 37 shows the mean and standard error of the mean for measurements of the alveolar corner area with increasing fluid load. Figure 38 shows the distribution of measurements for each fluid load. The Bonferoni Modified Student's t test for differences between the means found a significant change ($P < .05$) in the mean corner area between each fluid load. The distribution of corner area measurements showed the control and 10 percent load resulted in an approximately Gaussian distribution and the 30 and 50 percent loads resulted in a dispersed distribution. Thus, the corner area increased with increasing fluid load and the dispersion in measurement increased for the higher fluid loads.

Figure 39 shows the mean and standard error of the mean for alveolar cross-fractured width measurements with increasing fluid load. Figure 40 shows the frequency distribution of the width measurements for each fluid load. The Bonferoni Modified Student's t test for differences between the means showed no difference ($P > .05$) between the depth measurements of any two groups. The distribution of measurements and standard error of the mean indicate the dispersion of the measurements was approximately the same for all fluid loads.

Figure 41 shows the mean and standard error of the mean for alveolar cross-fracture depth measurements with increasing fluid load. Figure 42 shows the distribution of depth measurements at each fluid load. The Bonferoni Modified Student's t test for differences between the means showed no differences ($P > .05$) in alveolar width measurements between any two dogs. The distribution and standard error of the means showed a consistant dispersion of values between control and all experimental dogs.

DISCUSSION

Preservation by freeze-fixation with observation of the frozen-hydrated sample offers significant advantages in the study of fluid distribution in edematous lungs. Freeze-fixation permits monitoring of important physiological pressures such as P_{PA}, P_{LVED} and P_A at the moment of fixation. The alveolar space and alveolar fluids are preserved because in situ freeze-fixation maintains the integrity of the airway and pulmonary vascular systems. Observation of frozen-hydrated lung resulting from high-pressure pulmonary edema is useful because the pathological agent, water, is preserved. Correlated low temperature light and SEM observation is particularly well suited to the investigation of edematous lung tissue because light microscopy permits observation of large areas while SEM allows high resolution observation of three-dimensional alveolar structures. The new method of freeze-fracture, frozen-hydrated SEM observation of alveolar dimensions resulting from progressive high-pressure pulmonary edema were quantitated and correlated with pathophysiological, light microscopy and wet/dry lung weight ratio data in this study.

The pathophysiological data shows pulmonary vascular pressure increased by vascular overloading of 10, 30 and 50 percent body weight fluid loads in the experimental animals. Increased P_{PA} and P_{LVED} levels were seen with increased vascular fluid loads. The pulmonary vascular pressure increased 3 fold from baseline upon completion of the 10 percent body weight fluid load and increased 6 fold from baseline upon completion of 30 and 50 percent body weight fluid loads. Within

a half hour of completing fluid loading pulmonary vascular pressures returned to approximately normal values which indicated steady state vascular pressures had recovered before freeze fixation.

The pulmonary artery and left ventricle pressures represent the pulmonary pressure but it is the microvascular hydrostatic pressure (P_{MV}) which is actually the hydrodynamic pressure that forces the fluid out of the capillaries (Staub, 1974). Further, as a result of gravity, the P_{MV} varies over the height of the lung being the greatest at the lower portion of the lung and least at the higher portion of the lung (West et al., 1965). This distribution is consistent with the observation that edema development is more extensive in the lower lung. None the less, an average P_{MV} is useful and has been estimated by Gaar (1967) by the formula

$$P_{MV} = P_{LVED} + .4\ (P_{PA} - P_{LVED})$$

where .4 is the fraction of total pulmonary resistence downstream from the microvascular exchange site. This formula is a reasonable estimation based on the experimental measurements made by Bhattacharya and Staub (1979) which showed almost 50 percent of the total pulmonary pressure drop is along the alveolar capillary network. Using this estimate, for the average P_{MV} the change in P_{MV} (ΔP_{MV}) has been calculated from $\Delta P_{MV} = P_{MV}$ (after fluid load)--P_{MV} (before fluid load) for each animal.

In addition to the P_{MV}, the osmotic pressure in the microvascular vessels influences the uptake of water into the vascular system. The osmotic pressure of the systemic system is probably identical to the osmotic pressure within the lungs (Staub, 1974). Normal blood osmotic pressure is approximately 280 mosmoles, primarily generated from salts in solution with 1 mosmole due to proteins. Fluid loading of normal saline resulted in a change in systemic protein concentration in the 10, 30 and 50 percent body weight fluid loads. Landis and Pappenheimer (1963) have determined an imperical equation relating vascular protein osmotic pressure (π_{MV}) to protein concentration. For blood proteins this relationship is:

$$\pi_{MV} = 2.1\ C + 0.16C^2 + 0.009\ C^3$$

where C is the concentration of protein in gm/100 ml. Using this relation for π_{MV} the change in π_{MV} ($\Delta\pi_{MV}$) has been calculated from $\Delta\pi_{MV} = \pi_{MV}$ (after fluid load)—π_{MV} (before fluid load) for each animal.

From the estimates of P_{MV} and π_{MV} the total intravascular pressure (P_{IV}) at the end of fluid load has been calculated from:

$$P_{IV} = P_{MV} - \pi_{MV}$$

for each animal, From the estimates of ΔP_{MV} and $\Delta\pi_{MV}$, the change in total intravascular pressures (ΔP_{IV}) at the end of fluid load from before fluid load has been calculated from:

$$\Delta P_{IV} = \Delta P_{MV} - \Delta \pi_{MV}$$

for each animal. The values of ΔP_{MV}, $\Delta \pi_{MV}$, and ΔP_{IV} for control and fluid loaded animals have been summarized in Table 3.

TABLE 3

Calculated Changes in Microvascular Pressures with Fluid Loading

Fluid Load (percent body weight)	ΔP_{MV}	$\Delta \pi_{MV}$	ΔP_{IV}
	(CM H_2O)		
Control	0	0	0
10	12	5	7
30	37	14	23
50	38	15	25

Note: see text for discussion of values.

From this data it was concluded that the 10 percent body weight fluid load resulted in moderately elevated vascular pressure and 30 and 50 percent body weight fluid loads caused very high vascular pressure.

Wet/dry lung weight ratios agreed with those obtained by Guyton and Lindsey (1959) for fluid loaded dogs. There was no difference in the ratios between control and 10 percent body weight fluid loaded animals indicating this method was not sensitive enough to detect small amounts of edema. However, the control dog had a higher wet/dry ratio than the expected 3.5 (Staub, personal communication). This was probably the result of experimental error determining the wet/dry ratio for the animal because the lung appeared normal by histological criteria.

Low temperature light microscopy demonstrated the characteristic development of perivascular fluid cuffs around blood vessels and airways as described from light microscopy by Staub et al (1967) in response to fluid loading. The 10, 30, and 50 percent body weight fluid loaded animals showed an increasing accumulation of fluid in the perivascular cuffs. The light microscopy was sensitive to small amounts of edema and indicated that the induced pulmonary edema was progressive. This progressive nature was confirmed by the present low temperture SEM studies.

Low temperature SEM data from progressive high pressure pulmonary edema showed the fluid accumulated in alveolar walls and corners. The mid-alveolar cross fracture wall width of the normal lung was determined to be 3.5 μm. Fluid loading 10 percent body weight resulted in a wall width of 6 μm which was significantly ($P < .05$) different from normal wall width. Fluid loading 30 and 50 percent body weight also significantly ($P < .05$) increased wall width from normal but was not significantly thicker than the 10 percent body weight fluid load. Alveolar corner area measurements indicated a continuous significant ($P < .05$) increase in corner fluid accumulation with increasing fluid load. The thin, smooth alveolar walls from control lung defined polyhedrial shaped gas spaces. Moderately high pressure edema resulted in thick, undulating alveolar walls which defined polyhedrial gas spaces but with rounded corners. The undulating walls may result from fluid swelling the alveolar capillaries. High pressure edema caused more fluid to accumulate in the alveolar corners which resulted in spherical gas spaces.

The average cross fracture alveolar width for control lung measured 91 μm. All fluid loads resulted in a cross fractured alveolar width of approximately 83 μm. The 8 μm decrease in cross fractured alveolar width between control and edematous lungs is explained by the increase of 3 μm alveolar wall width on each side of the alveolus (6 μm total) between control and edmeatous lungs. The average alveolar cross-fracture depth of control lung measured 52 μm while the average alveolar cross fracture depth of all fluid loaded lungs measured 46 μm. The difference in average alveolar depth between edematous and control lung is approximately explained by an increase of 3 μm in alveolar wall width between edematous and control lungs. The average normal alveolar width measurement of 91 μm obtained by freeze-fracture, frozen-hydrated SEM is in agreement with that obtained by Staub (1967) of 100 μm diameter determined by light microscopy. Further the constant alveolar width and depth measurements in moderate and severe edematous lungs supports the hypothesis that the alveolar gas space decreases to a critical minimum radius of curvature before flooding occurs (Staub, 1967). This hypothesis is based on "quantum" alveolar flooding where individual alveoli flood independently and completely when the gas space reaches a critical radius of curvature and the airway pressure is no longer able to support the alveolar air space.

From the low temperature SEM data and the pathophysiological data a model of alveolar fluid accumulation resulting from progressive high pressure edema was determined. Moderate high pressure results in

fluid accumulation in alveolar walls and corners (presumably in the interstitial spaces), and causes distention of the alveolar surface above the capillary network. High pressure causes accumulation of fluid in alveolar walls and corners, causes the alveolar gas space to assume a spherical shape. This mode is diagrammed in Figure 43.

The methodology of frozen hydrated SEM lung observation developed in this dissertation will be useful in studying lung structure and lung pathology because it preserves pulmonary fluids and gas spaces in situ and important physiological information can be obtained at the moment of freeze fixation. The preservation of lung fluids and gas spaces in the frozen-hydrated state results in a minimum of fluid redistribution and permits SEM analysis of delicate alveolar structure. Combining low temperature SEM with microdissection of airways at low temperature (Bastacky et al., 1980) with low temperature SEM will allow observation of fluid distribution along our airway which would be a useful approach to study the hypothesis that the site of alveolar flooding may be along the terminal airways (Staub, 1979). The new metnod of freeze-fracture, frozen-hydrated, SEM lung preservation allows unique new opportunities to study lung pathology.

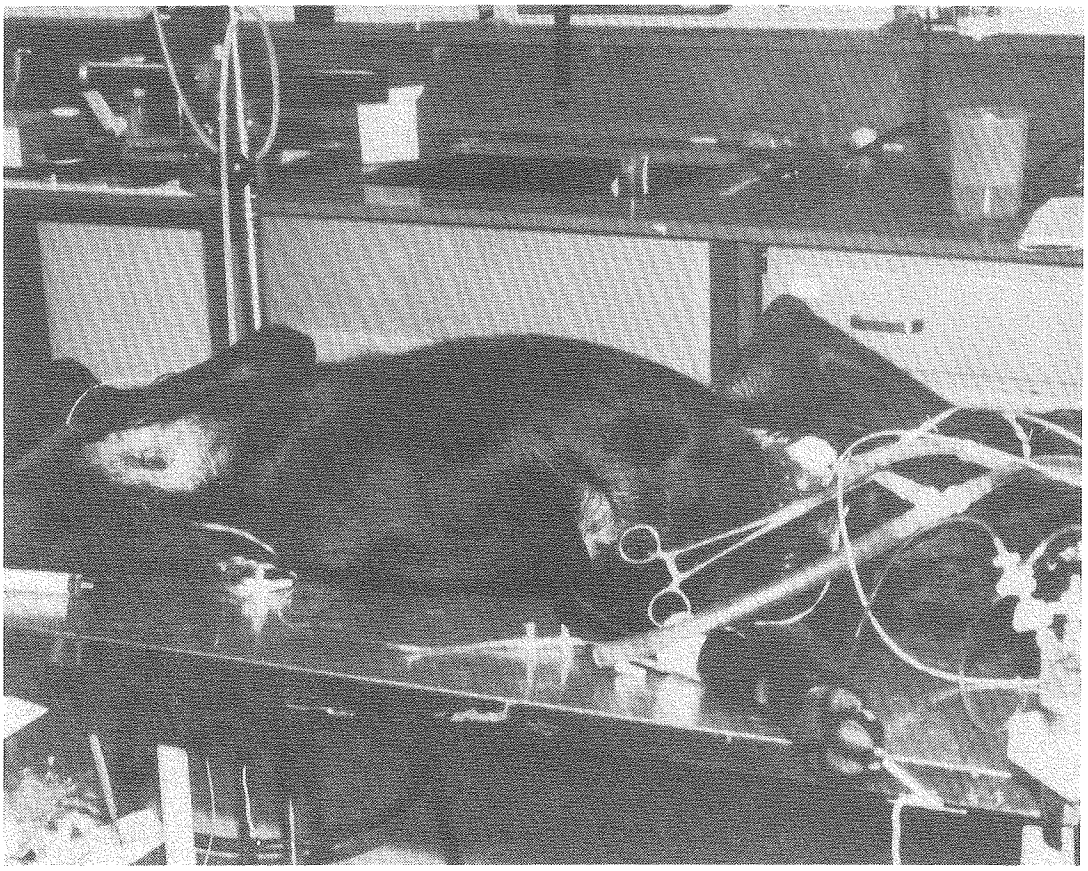

Figure 1. A right lateral photograph of an experimental dog with airway ventilation tubing and catheters in the pulmonary artery, left ventricle, femoral artery and femoral vein. The dogs were deeply anesthetized during experimental procedures and careful animal surgical techniques were applied. (CBB 8012-14274)

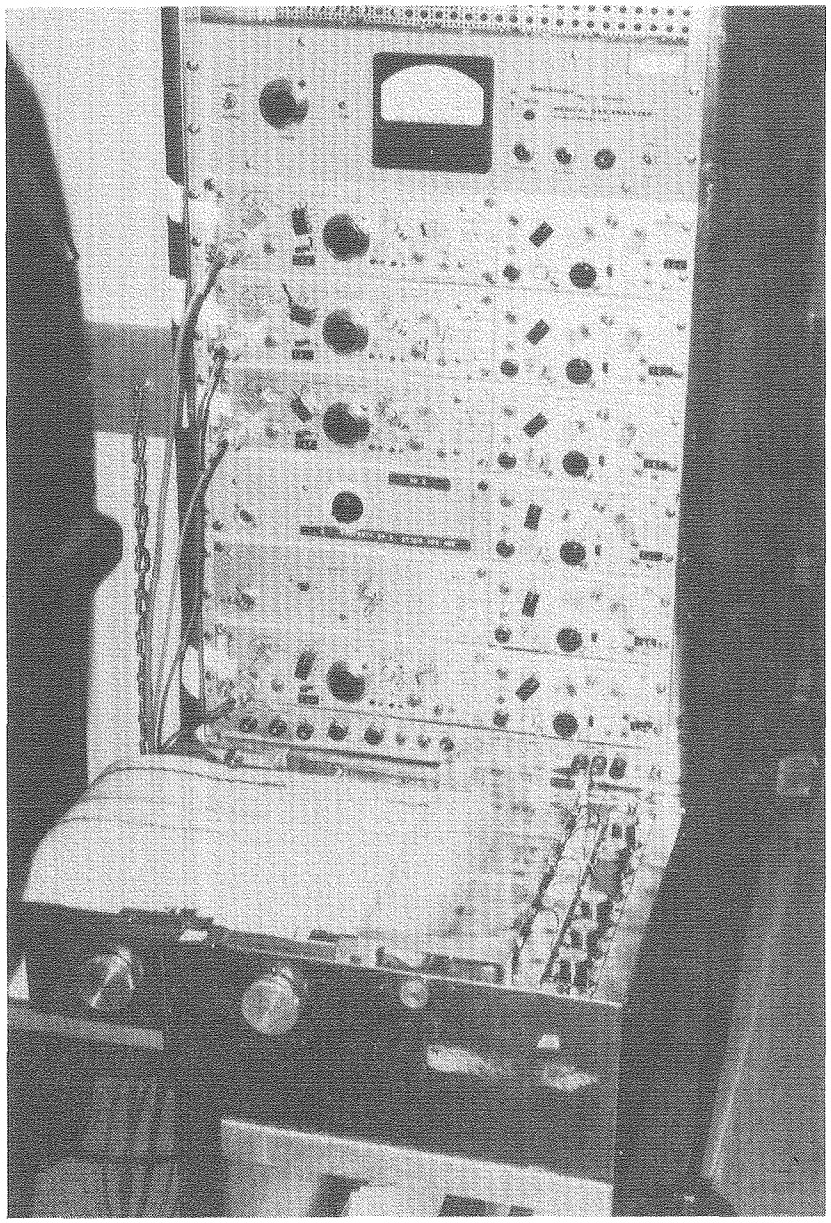

Figure 2. Photograph of the polygraph multichannel amplifiers and strip chart recorder (Grass Model 7) used to amplify and record strain gauge measurements of airway, pulmonary artery, left ventricular endiastolic pressure and systemic blood pressures. (CBB 8012-14276)

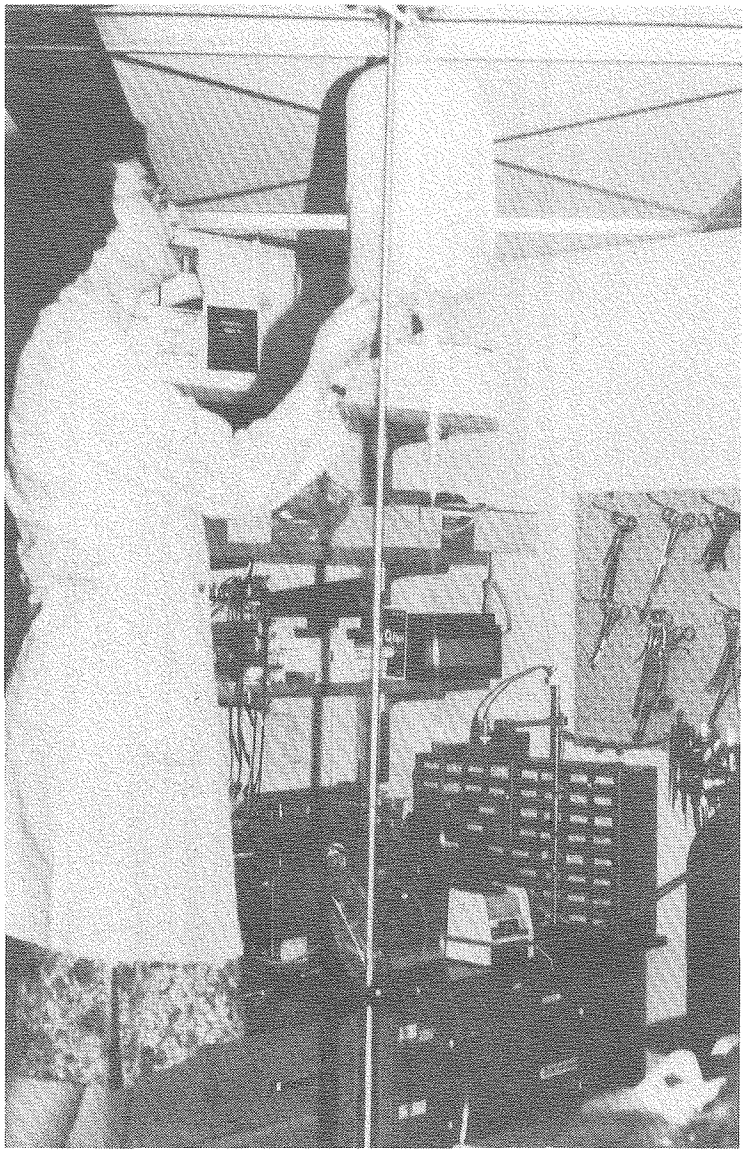

Figure 3. Photograph of normal saline fluidload at a height above the dog to achieve a fluid load of 1 percent body weight min. (CBB 8012-14284)

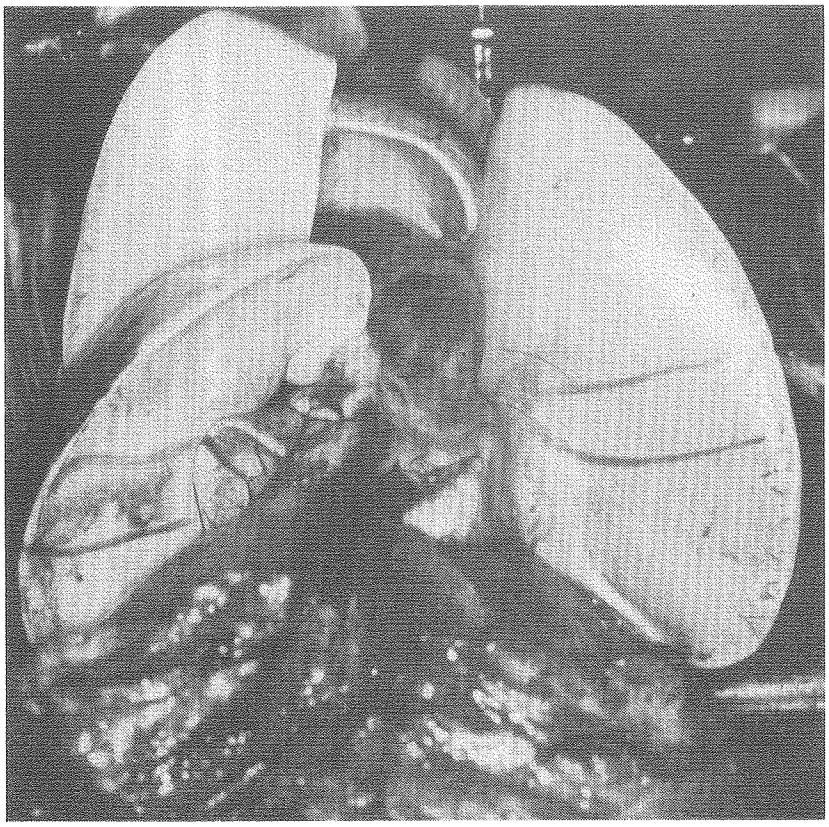

Figure 4. A caudal-caphalic photograph of inflated lungs in the open chest cavity of the dog. The parallel lines, spaced 2.5 cm apart, were drawn on the diaphramatic surface of the left and right lower lobes. This defined the height of the lung of the tissue used for low temperature LM and SEM observation. SEM samples were of alveoli .5-1.5 mm in from the diaphramatic pleural surface area defined by the marking lines on the right lower lobe. (CBB 8012-14282)

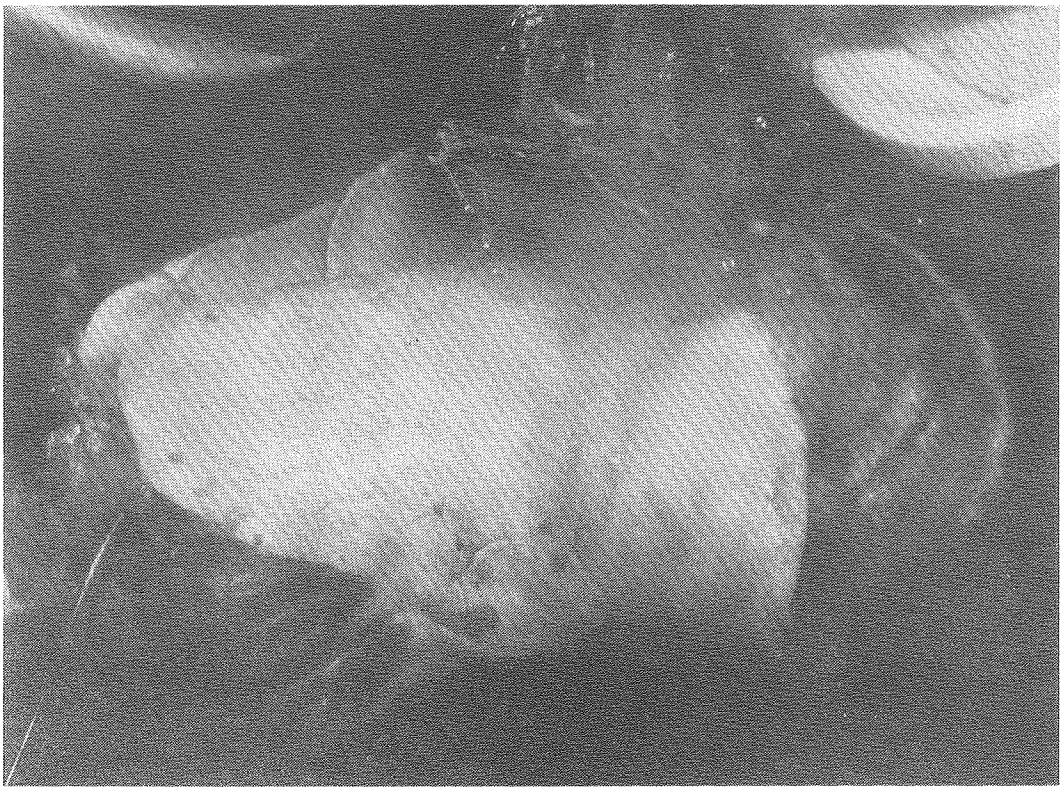

Figure 5. A lateral photograph of inflated lungs in the open chest cavity at the moment of freeze fixation. The freezing was achieved by pouring liquid nitrogen (LN_2) onto the inflated lung *in situ*. (CBB 8012-14292)

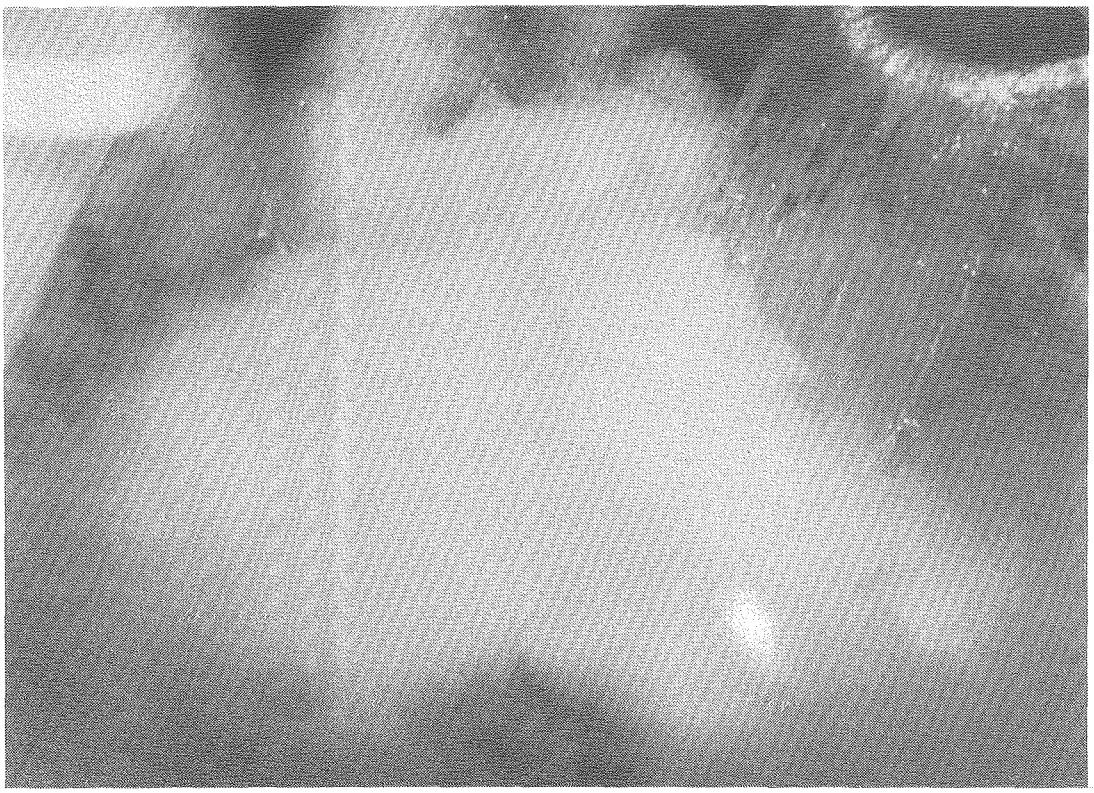

Figure 6. A photograph of liquid nitrogen being poured on the inflated lung. The cloud is the condensed atmospheric water vapor cooled to the dew point by LN_2. CBB 8012-14280

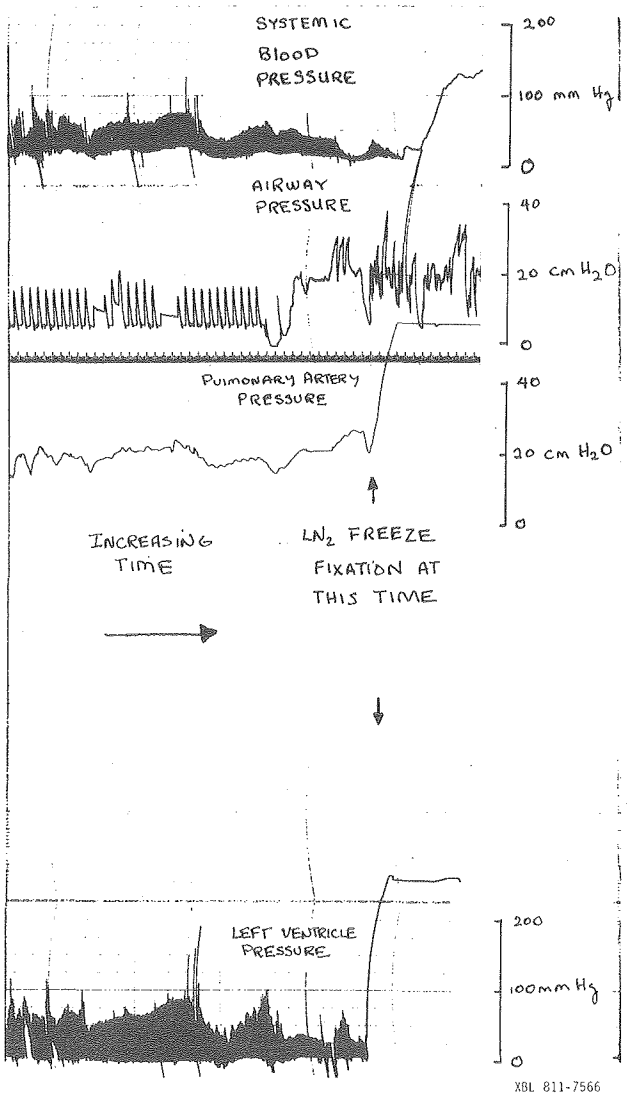

Figure 7. A strip chart recording documenting the systematic blood pressure, airway pressure, pulmonary artery pressure and left ventricle pressure at the moment of freeze fixation.

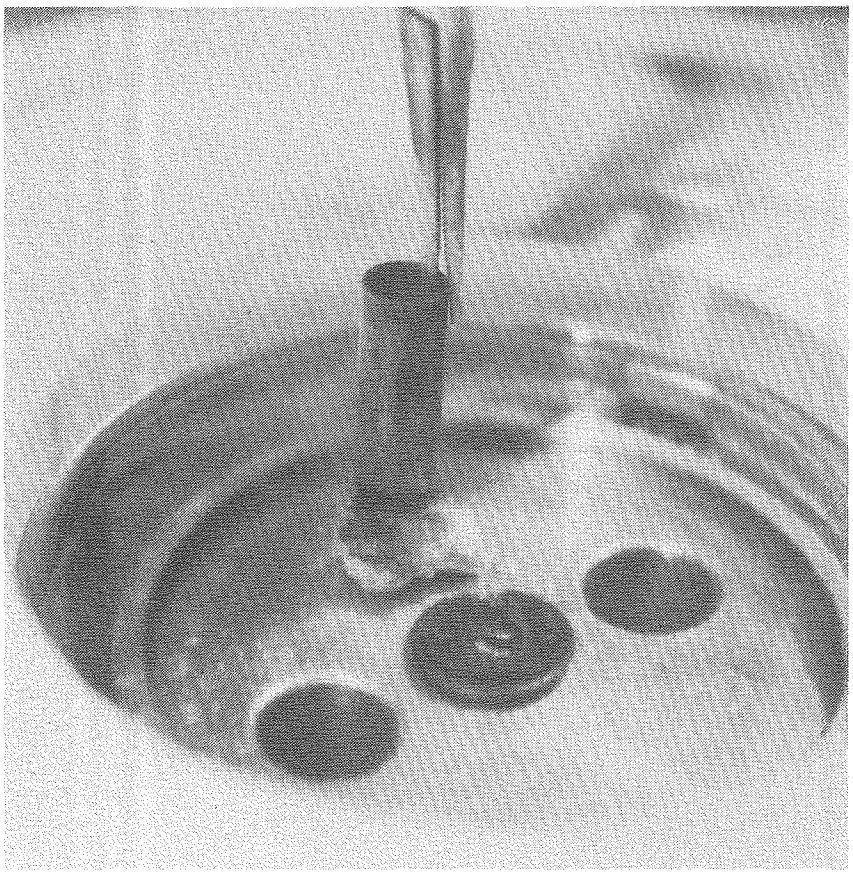

Figure 8. A photograph of the low temperature sample mounting platform. An aluminum platform is suspended in LN_2 and a copper sample stub(s) threaded into it. A small piece of frozen lung from the marked region has been cut out of the lung under LN_2 and placed on the mounting platform under LN_2. A pre-cooled punch and hematostat was used to core bore a cylinder of frozen lung at right angle to the diaphramatic pleural surface. CBB 8012-14915

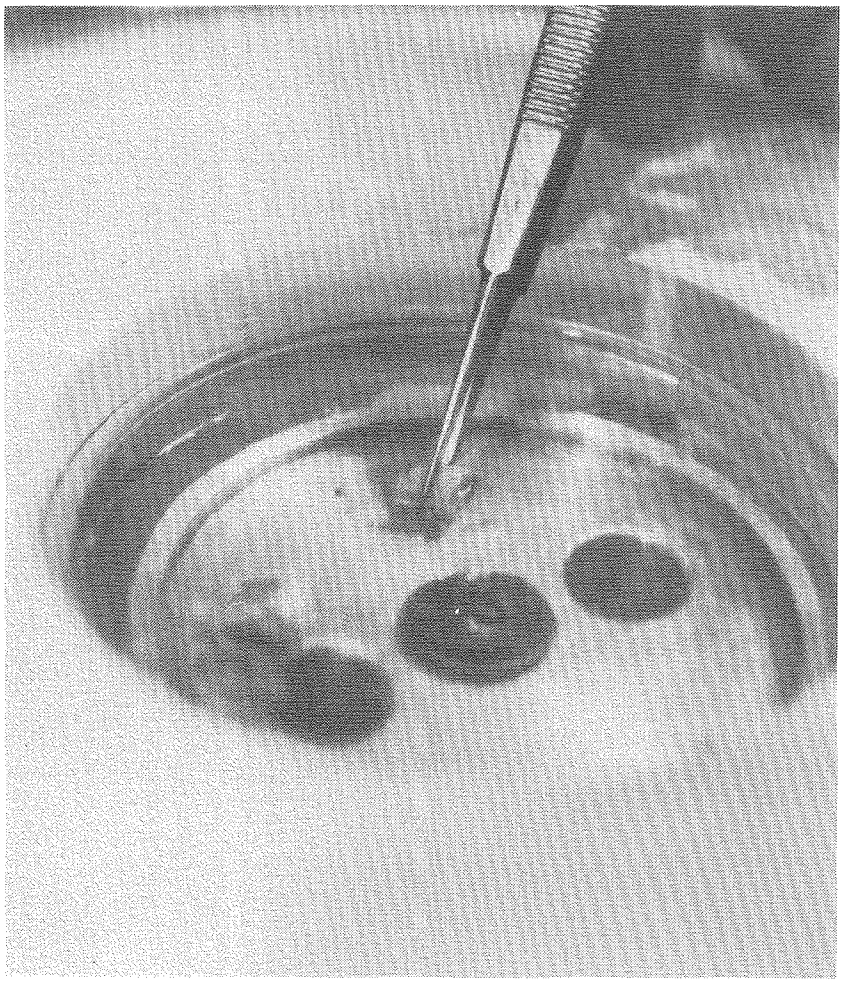

Figure 9. The frozen lung cylinder was removed from the punch and held with pre-cooled forceps at the surface of the LN_2. Note the blue diaphramatic surface colored by the blue marking paint. CBB 8012-14913

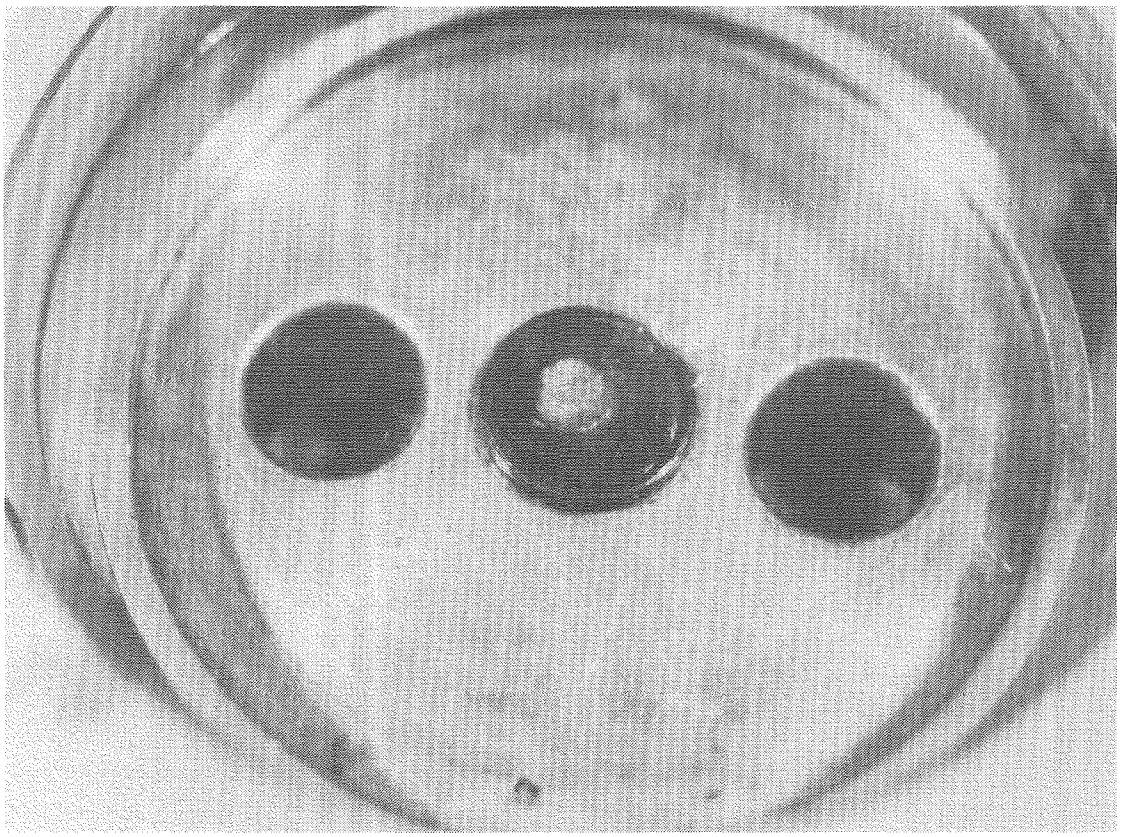

Figure 10. The frozen lung cylinder was mounted under LN_2 onto the copper sample stub with a sliding mechanical clamp. The pleural surface was placed down onto the stub. This stub held the sample during freeze-fracture and low temperature SEM observation. CBB 8012-14911

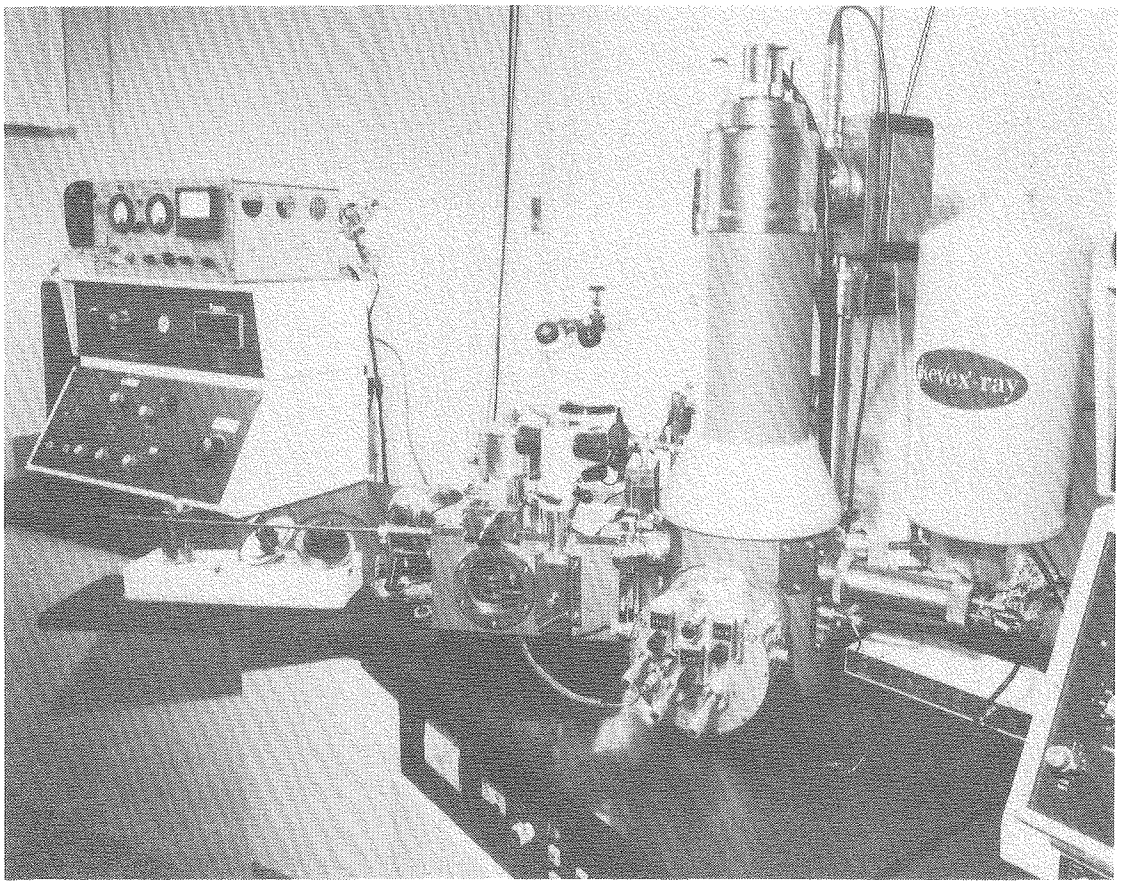

Figure 11. A photograph of the AMR Biochamber cryosample preparation chamber attached to the column of the AMR 100A SEM. The binocular light microscope allowed observation of the freeze-fractured lung before metal coating and SEM observation. CBB 7911-14712

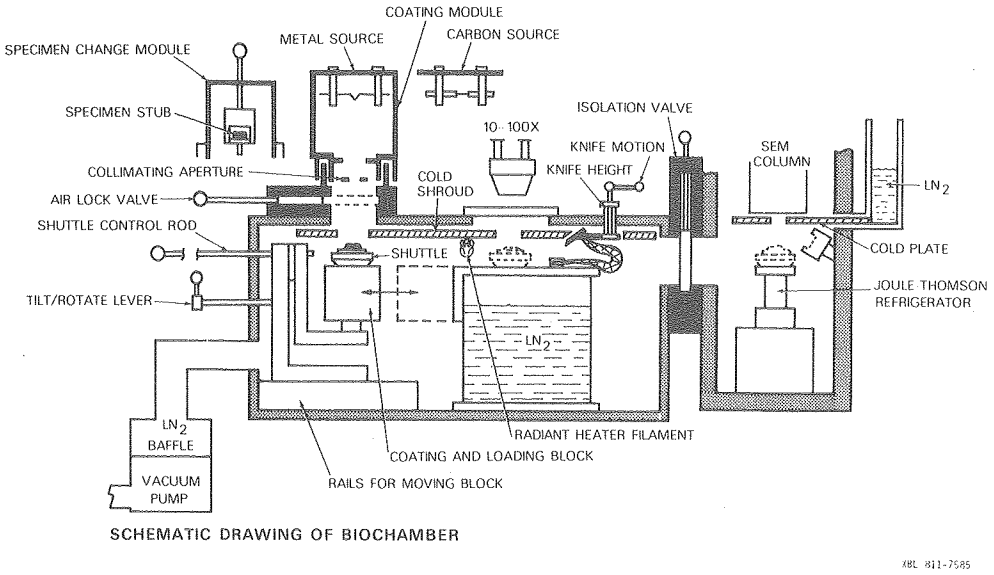

Figure 12. A line drawing of the Biochamber attached to the SEM column. The frozen sample and stub was rapidly transferred with the transfer module via the air lock into the low temperature, high vacuum environment of the cryosample preparation chamber where the lung was freeze-fractured and metal coated prior to SEM observation on the low temperature stage.

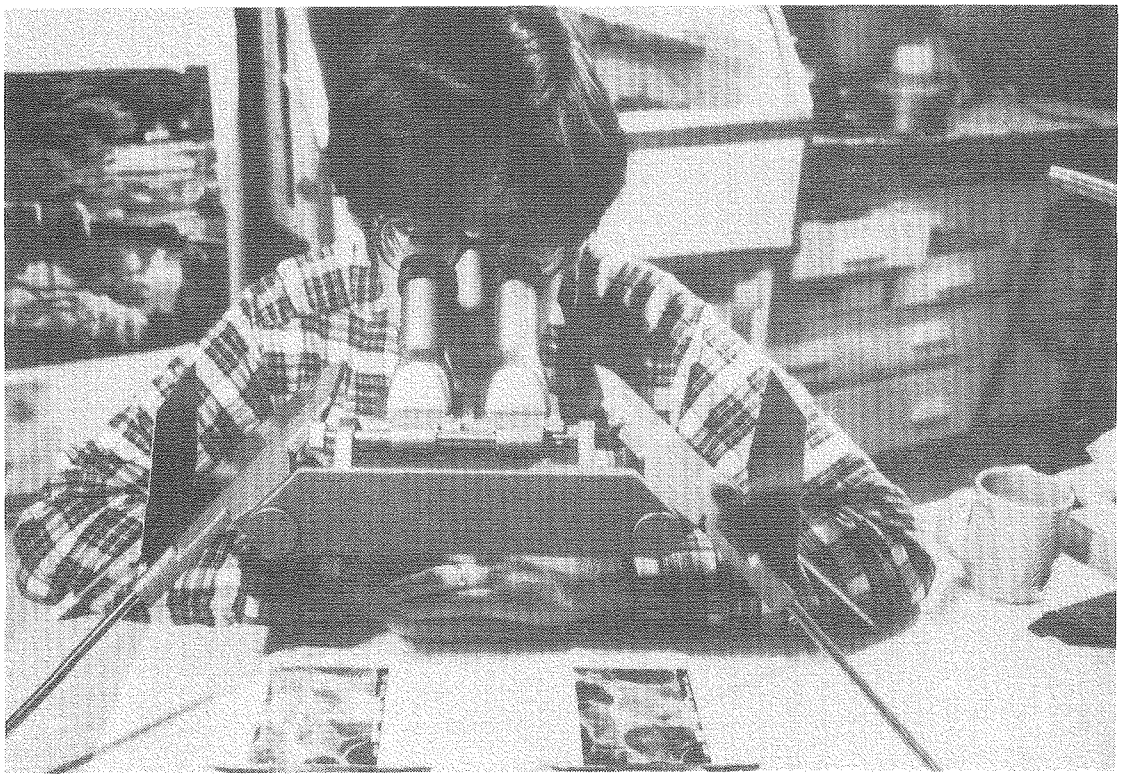

Figure 13. Photograph of author measuring stereopair SEM micrographs using a simple stereometer with 3X oculars and a calibrated reticle. CBB 8012-14907

PATHOPHYSIOLOGICAL PRESSURE ANALYSIS

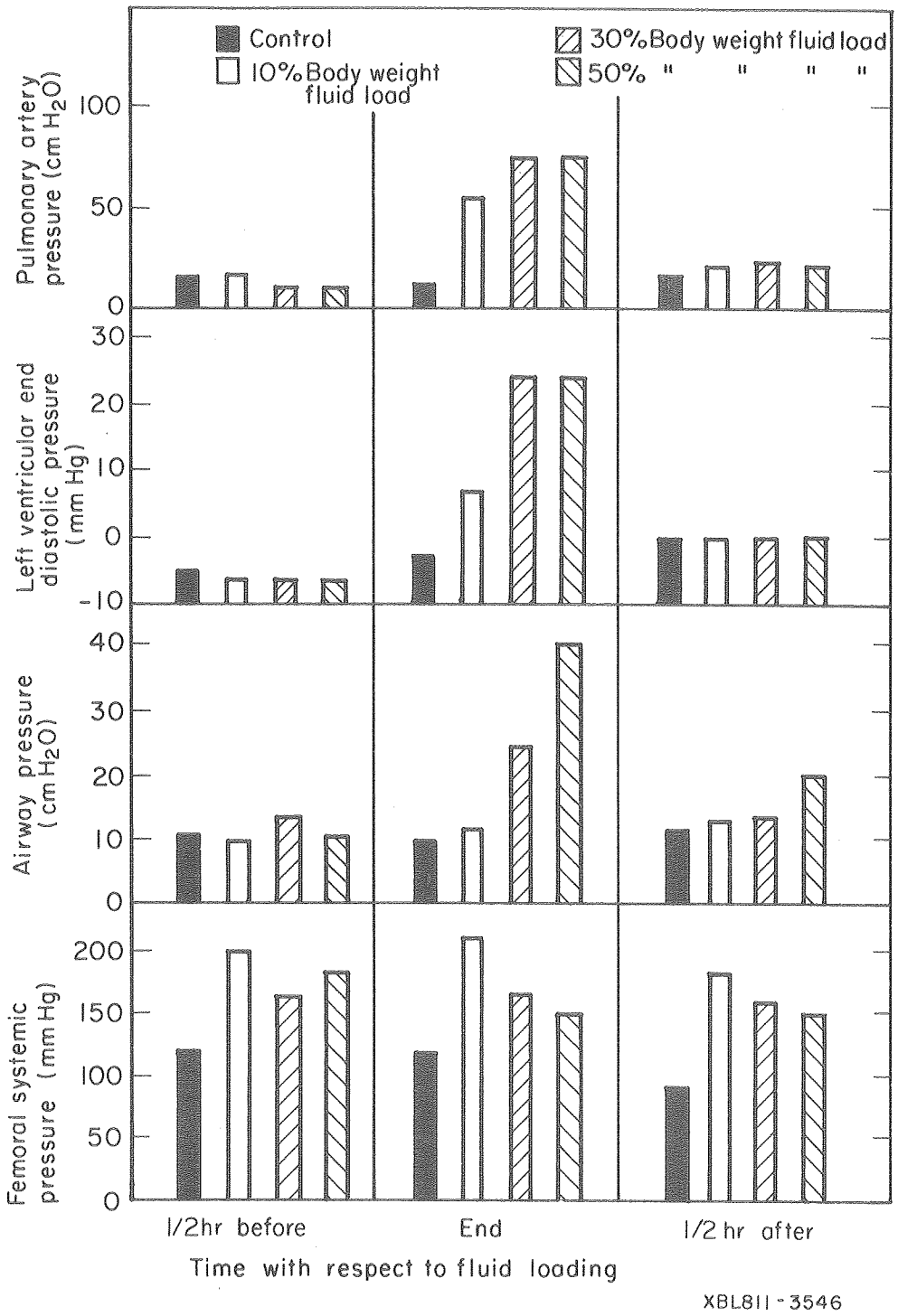

Figure 14. Pressure analysis obtained .5 hr before, at the end, and .5 hr after fluid loading for control, 10, 30, and 50% body weight fluid loads.

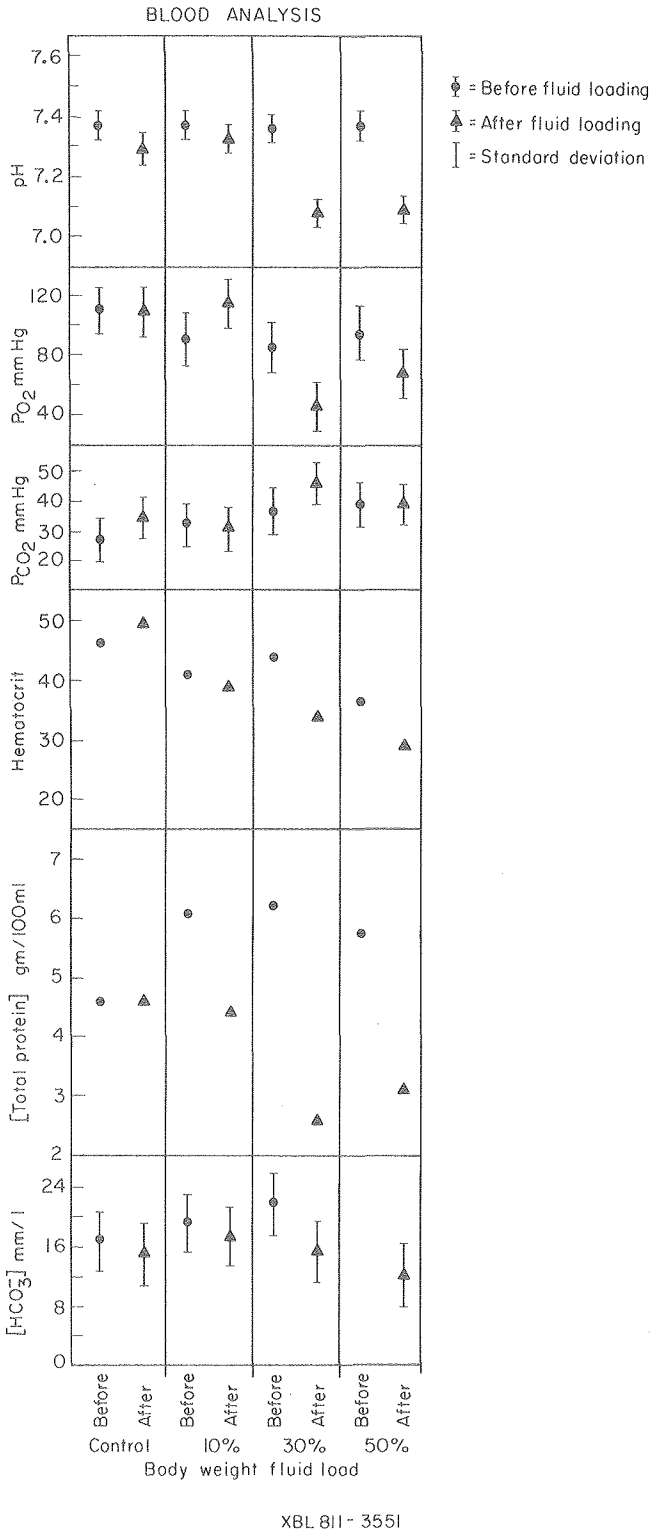

Figure 15. Blood analysis obtained before and after fluid loading for control, 10, 30 and 50% body weight fluid loads.

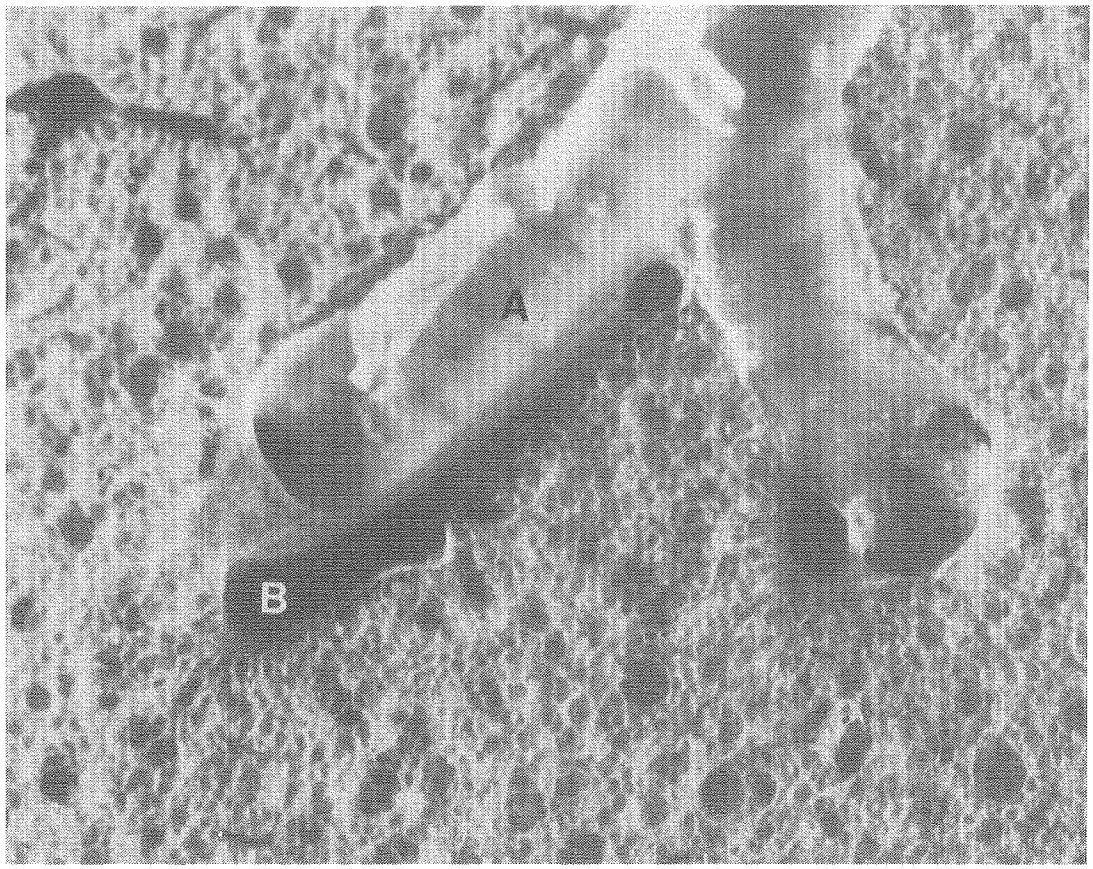

Figure 16. Control frozen lung light micrograph (magnification 20X). Note the thin walls surrounding airways (A) and blood vessels (B) and numerous open alveoli. CBB 800-14290A

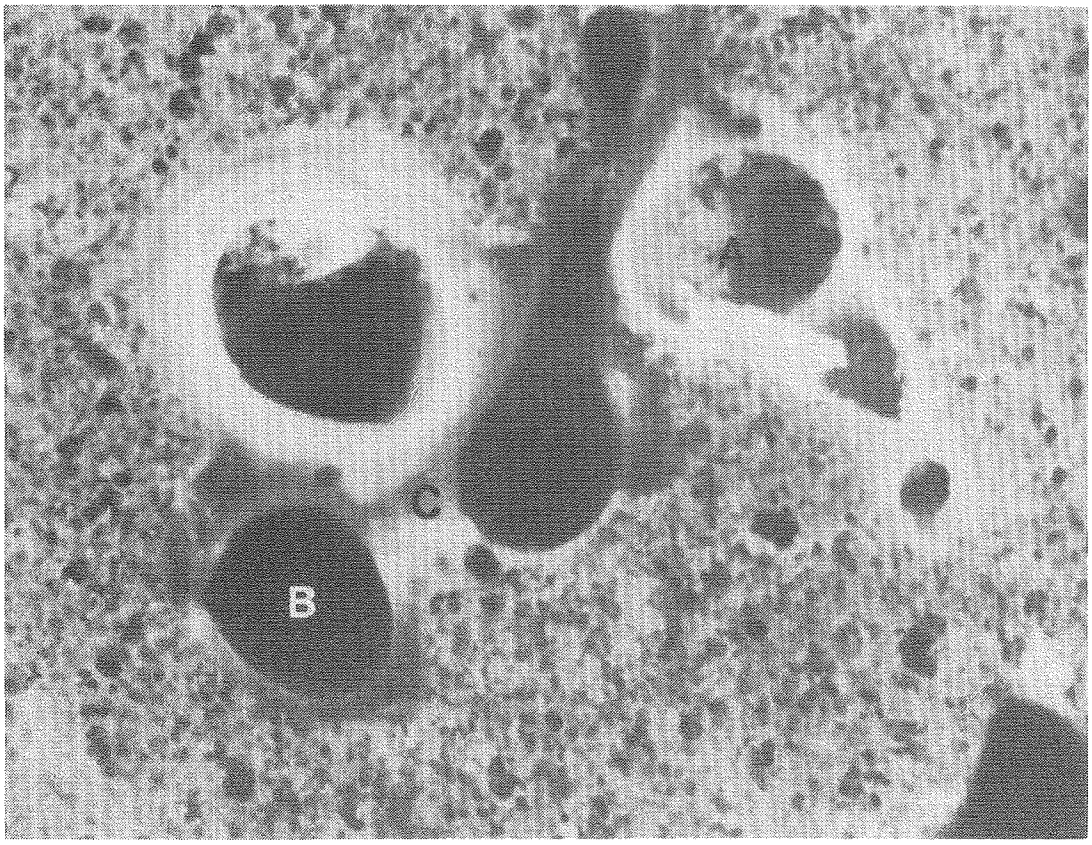

Figure 17. Ten percent fluid loaded lung light micrograph (magnification 20X). Note the appearance of perivascular fluid cuff (C) surrounding the airways (A) and the blood vessels (B). CBB 800-14288A

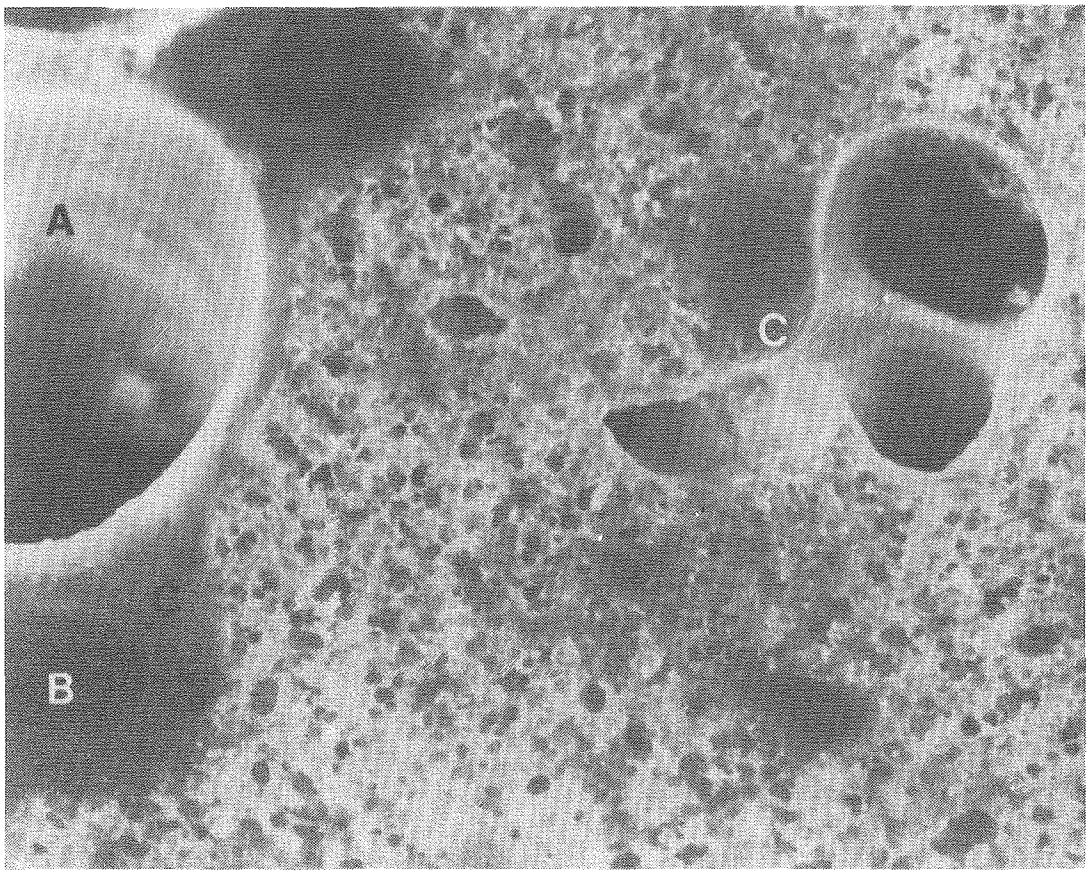

Figure 18. Thirty percent body weight fluid loaded lung light micrograph (magnification 20X). The perivascular cuffs (C) surround airways (A) and blood vessels (B). The red color of the cuff fluid indicates leakages of red blood cell fluid indicates leakage of red blood cells into the perivascular cuffs. CBB 800-14278A

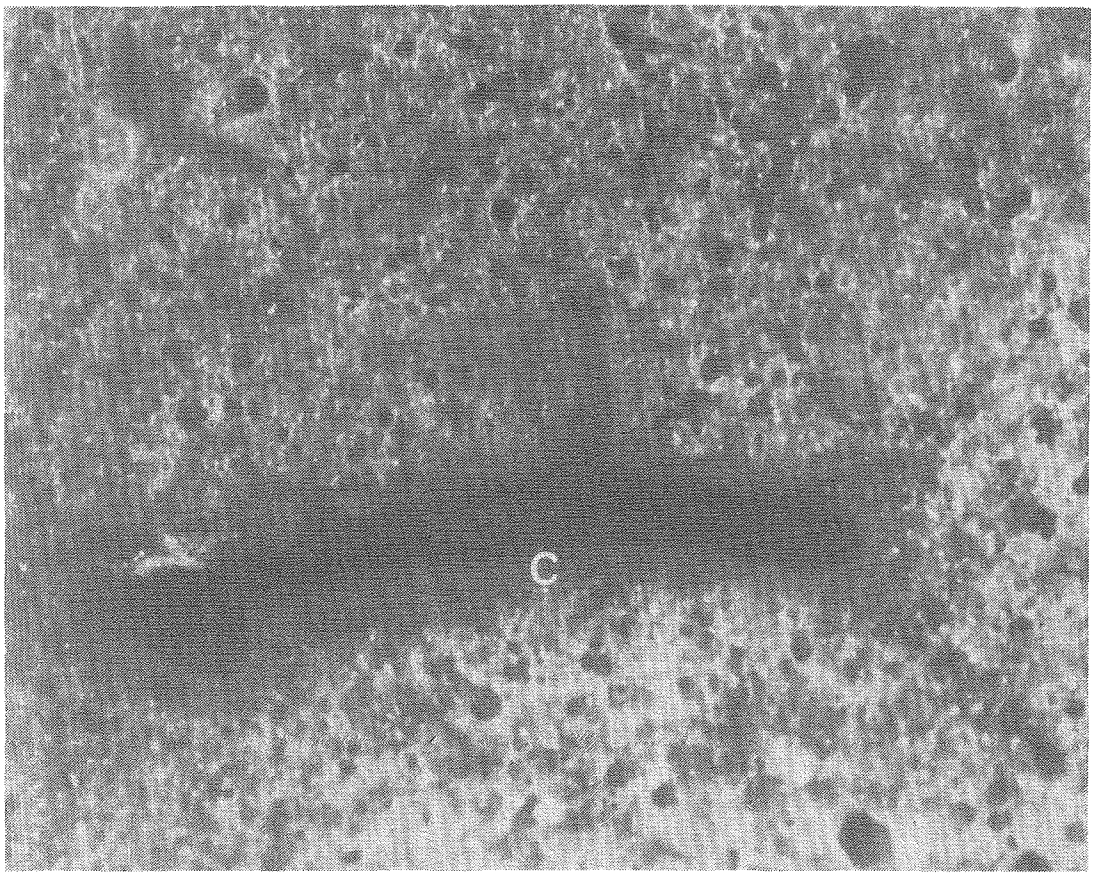

Figure 19. Fifty percent body weight fluid loaded lung light micrograph (magnification 20X). The extent of perivascular fluid cuff (C) formation is comparable to that developed in the thirty percent body weight fluid loaded lung. CBB 800-14286A

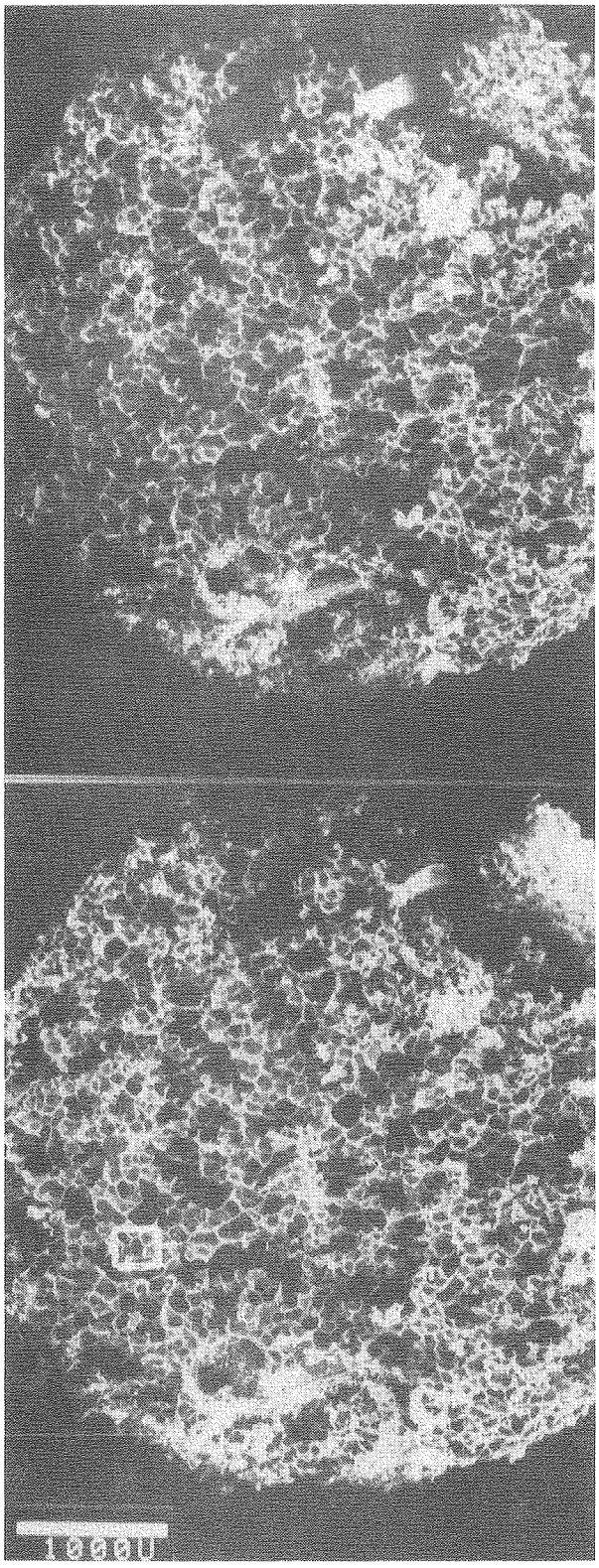

Figure 20. Freeze-fractured, frozen hydrated, Au coated SEM stereo micrographs of control lung (magnification 20X). Note the convoluted fractured surface and the boxed area showing the location in this micrograph of Figure 21.

XBB 800-13286A

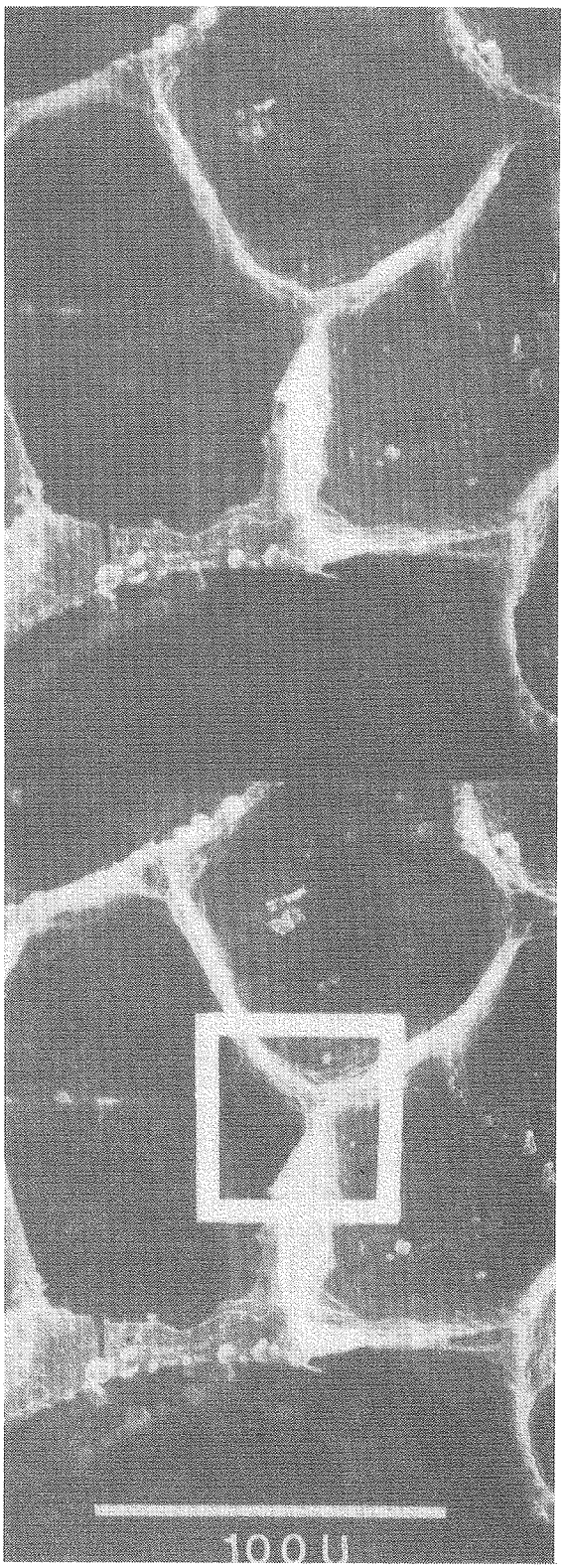

Figure 21. Freeze-fractured, frozen-hydrated, Au coated SEm stereo micrographs of control lung (magnification 500X). Note the thin, smooth, alveolar walls defining polyhedrial shaped air spaces. The boxed area shows in this micrograph the location of Figure 22. XBB 800-13354A

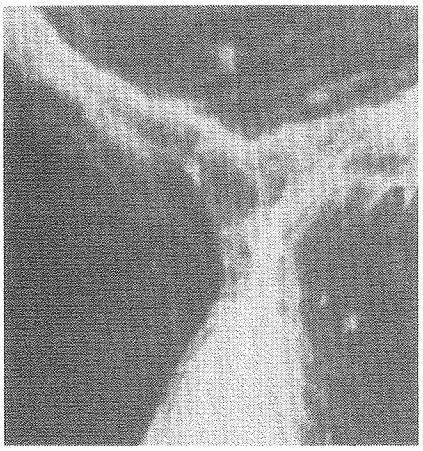

Figure 22. Freeze-fractured, frozen-hydrated, Au coated alveolar wall of control lung (magnification 1500X). This was the enlargement used to measure alveolar structures. XBB 800-13354B

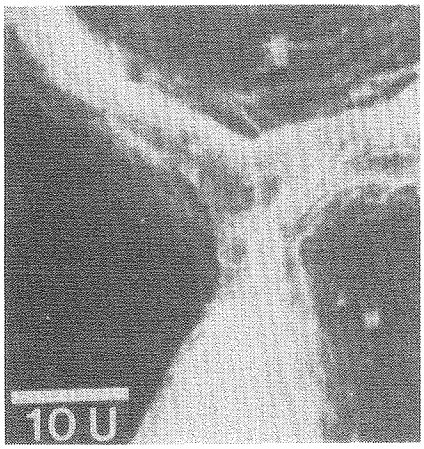

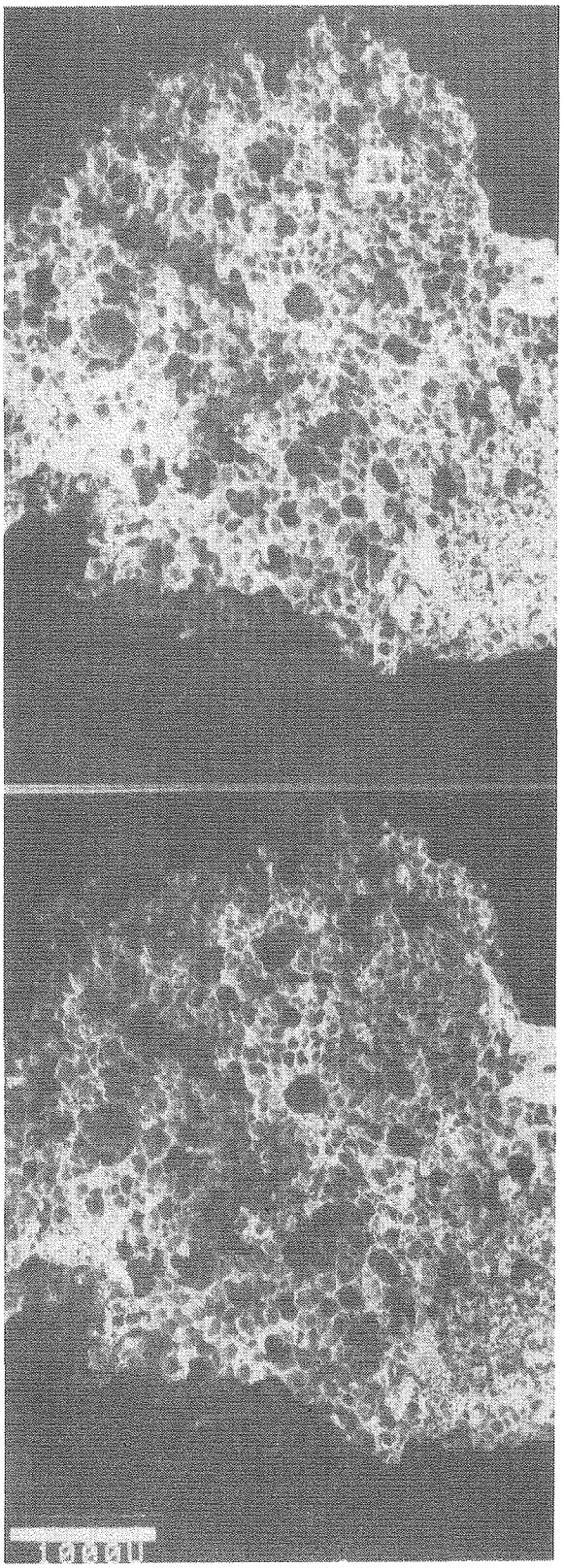

Figure 23. Freeze-fractured, frozen hydrated, Au coated, SEM stereo micrographs of lung from the 10% fluid load animal (magnification 20X). The box shows the location of Figure 24.

XBB 800-13097A

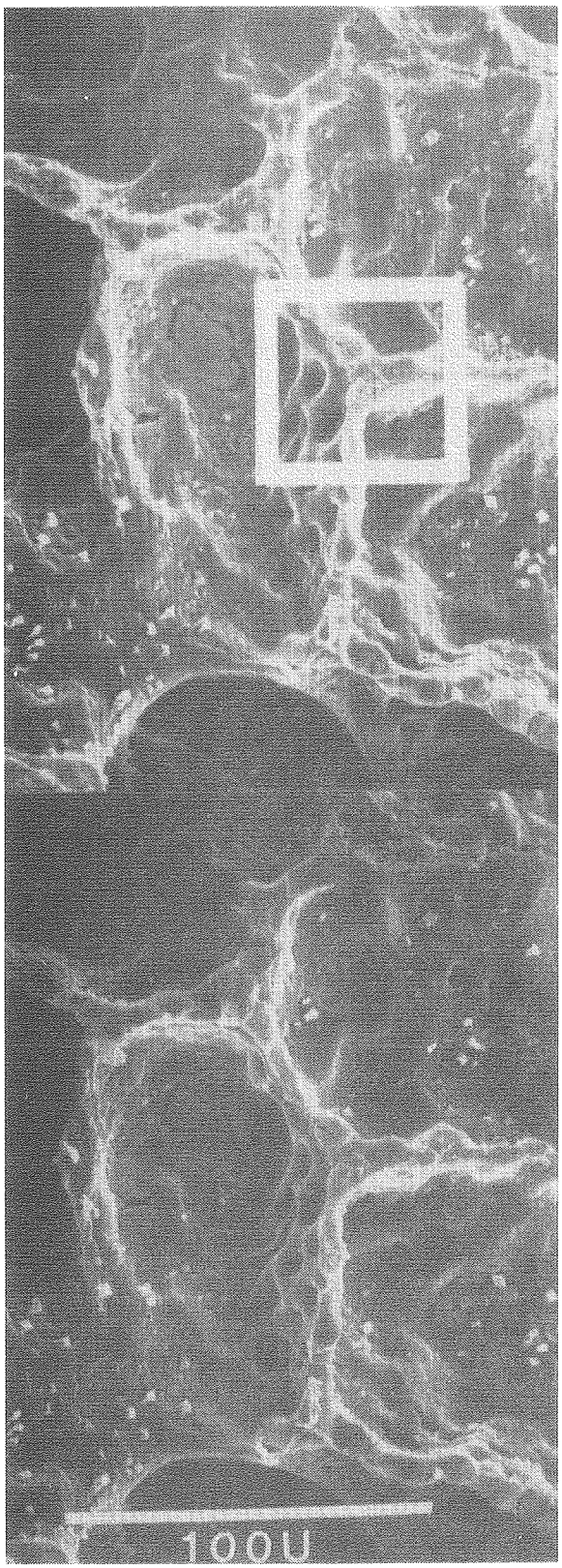

Figure 24. Freeze-fracture, frozen-hydrated, Au coated SEM micrographs of lung from the 10% fluid load animal (magnification 500X). Note the thick, undulating surfaces of the alveoli. The box shows the location of Figure 25.
XBB 800-13024A

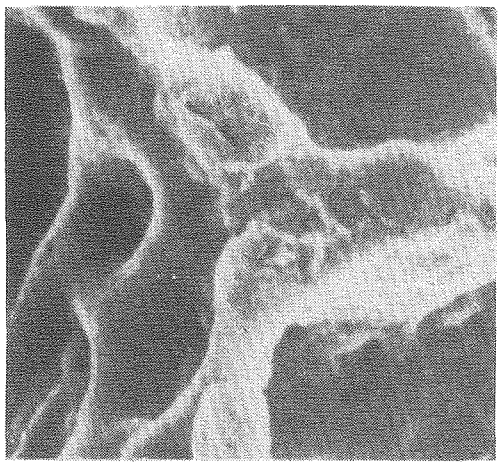

Figure 25. Freeze-fractured, frozen-hydrated, Au coated SEM stereo micrographs of alveolar wall from the 10% fluid load animal (magnification 1500X). This was the enlargement used to measure alveolar strucutres.

XBB 800-13024B

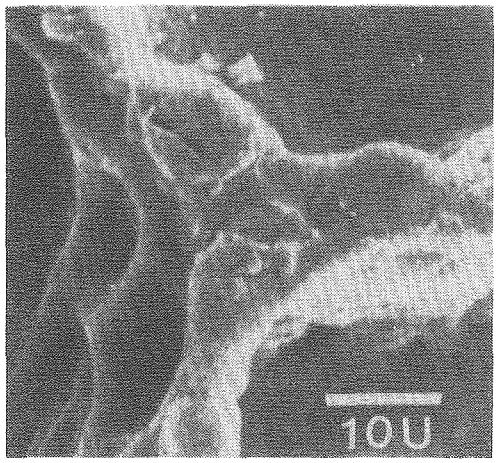

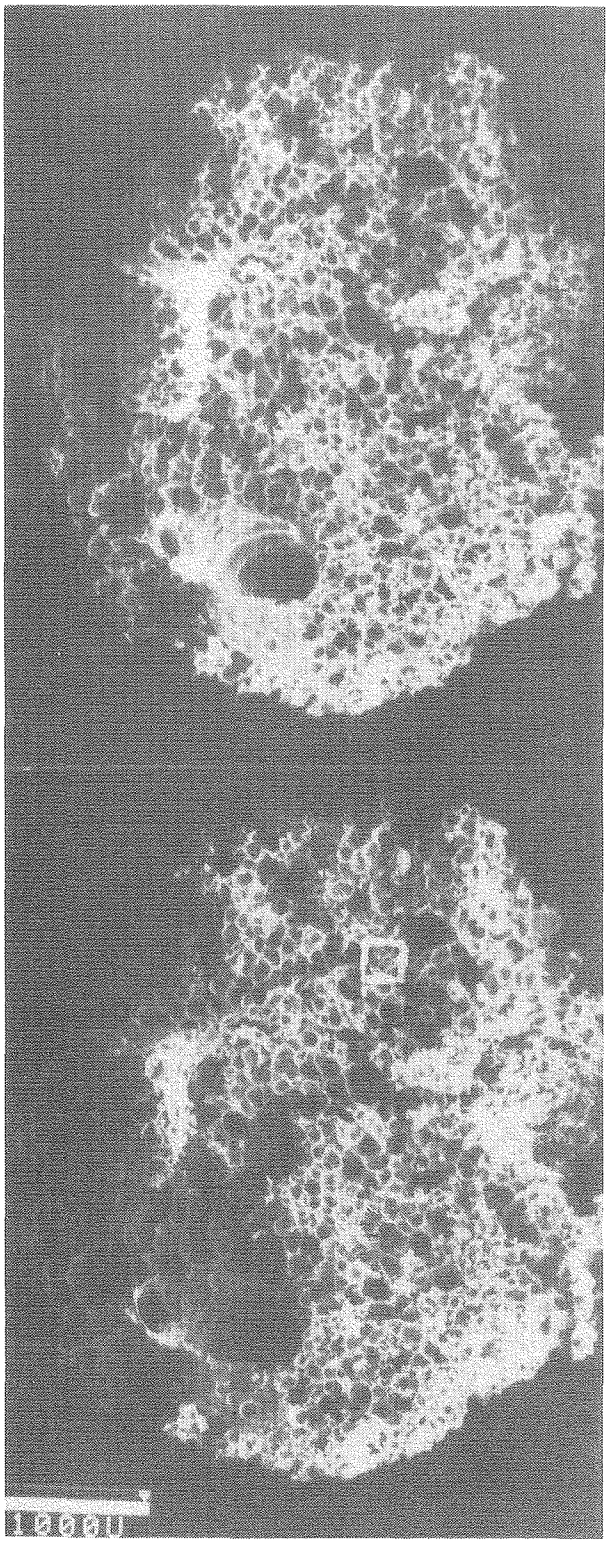

Figure 26. Freeze fractured, frozen-hydrated, Au coated SEM stereo micrographs of lung from the 30% fluid load animal (magnification 20X). The box defines the location of Figures 27. XBB 800-13145A

Figure 27. Freeze-fractured, frozen-hydrated, Au coated SEM stereo micrographs of lung from the 30% fluid load animal (magnification 500X). The box defines the location in Figure 28. XBB 800-13141A

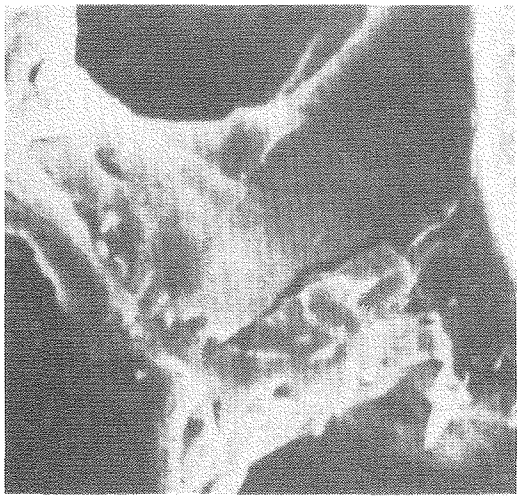

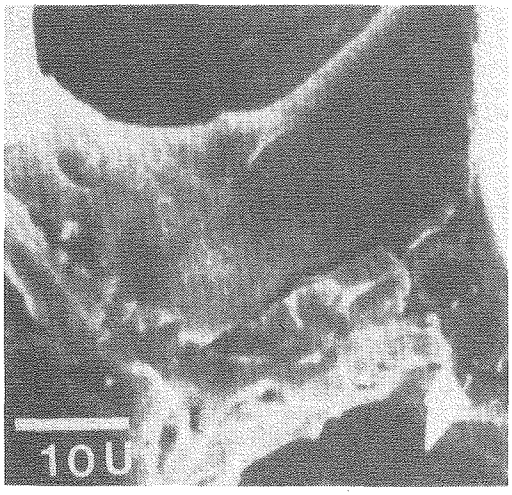

Figure 28. Freeze-fractured, frozen hydrated, Au coated SEM stereo micrographs of alveolar walls from the 30 percent fluid load animal (magnification 1500X). XBB 800-13141B

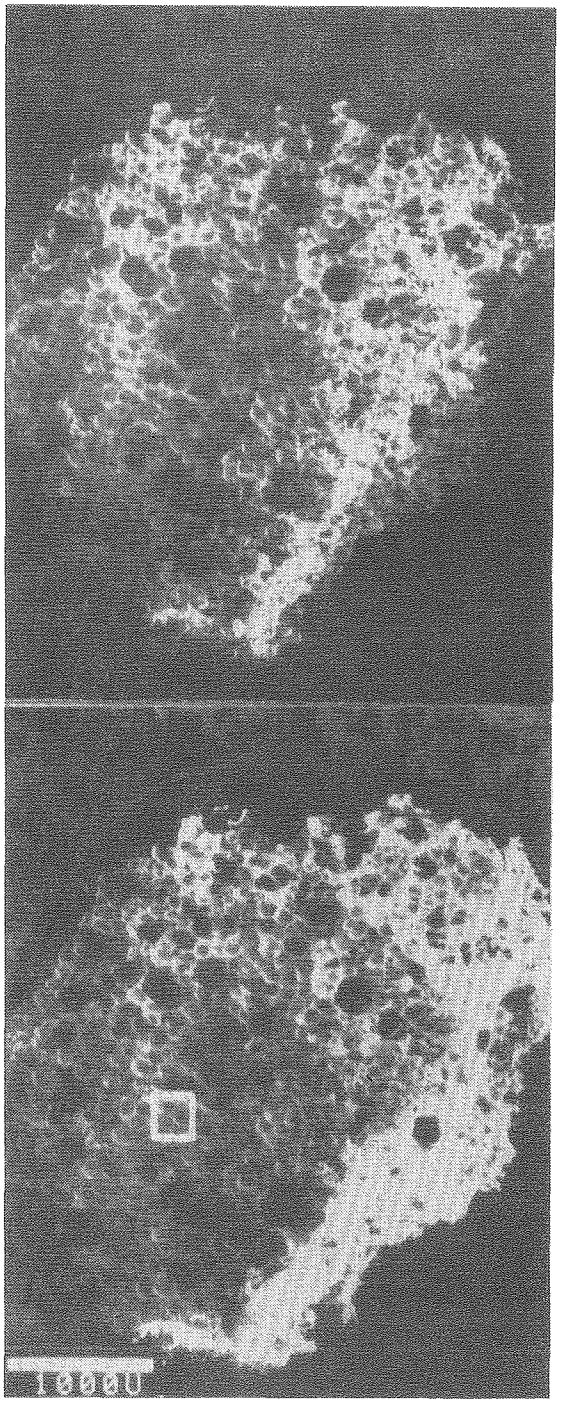

Figure 29. Freeze fractured, frozen hydrated, Au coated SEM stereo micrograph of lung from the 50 percent fluid load animal (magnification 20X). The box defines the location of Figure 30.

XBB 800-12979A

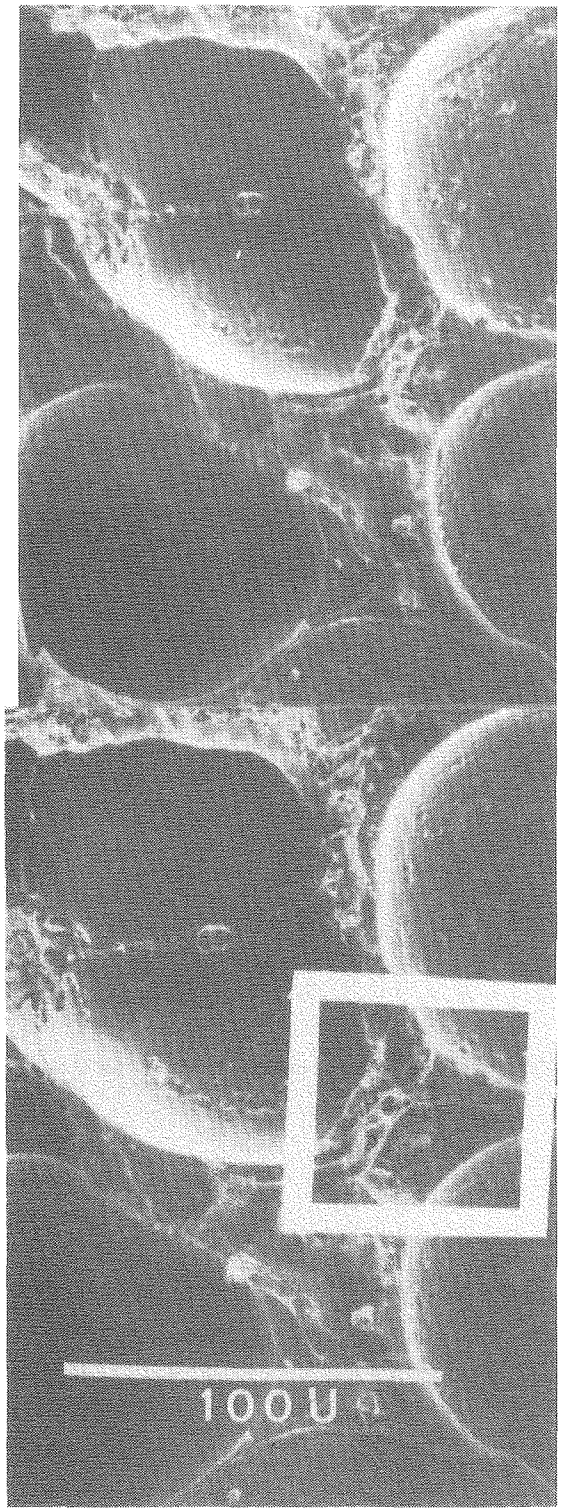

Figure 30. Freeze-fractured, frozen hydrated, Au coated SEM stereo micrographs of lung from the 50 percent fluid load animal (magnification 500X). Note the accumulation of fluid in the alveolar corners resulting in a spherical gas space. The box defines the location of Figure 31. XBB 800-13177A

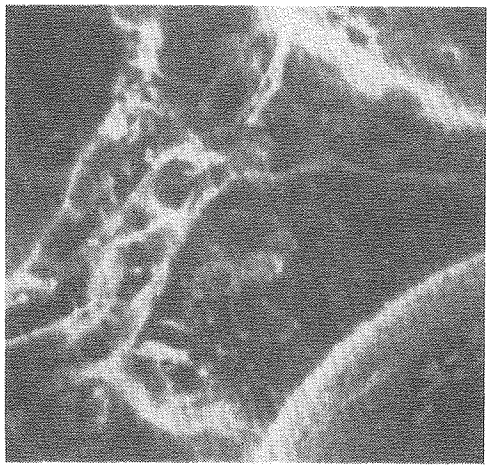

Figure 31. Freeze-fracture, Frozen hydrated Au coated SEM stereo micrographs of lung from the 50 percent fluid load animal (magnification 1500X). XBB 800-13177B

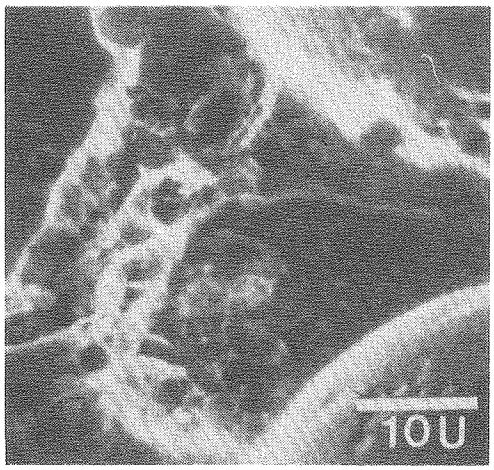

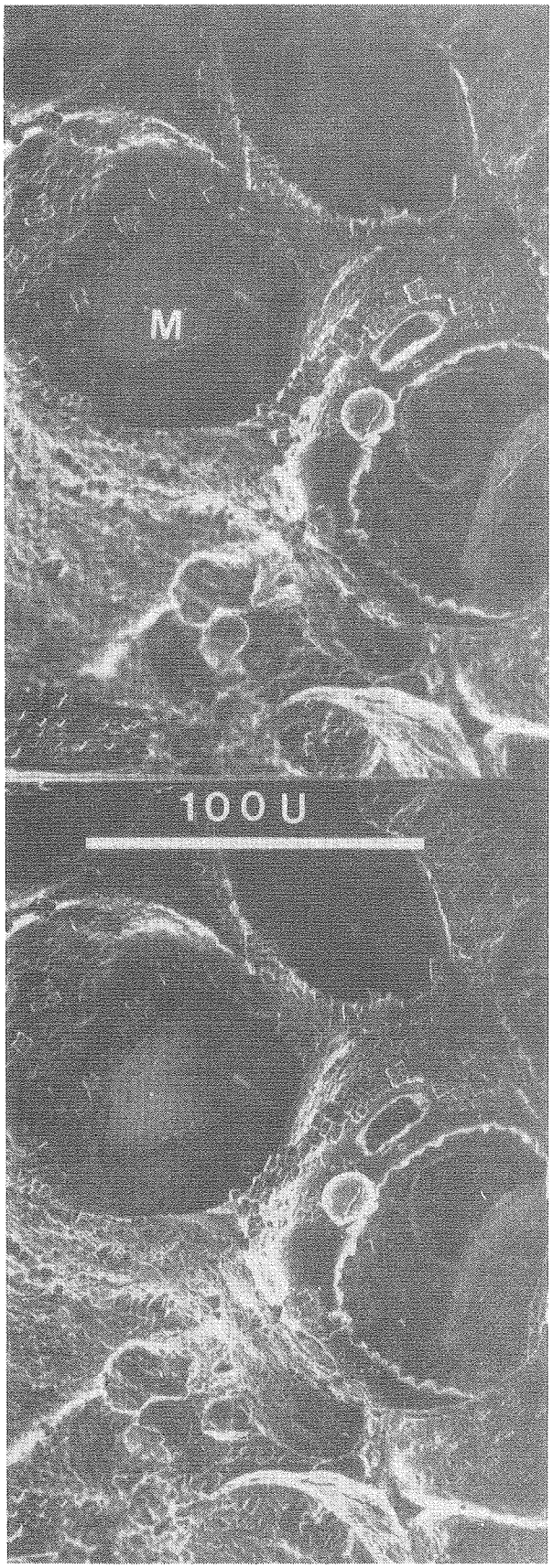

Figure 32. Freeze-fractured, frozen hydrated, uncoated SEM stereo micrographs (magnification 500X). Note the large membrane structures (M) across the alveoli. These structures were seen in every lung sample observed in low temperature SEM preserved in the frozen-hydrated state at a temperature below -140°C, XBB 800-13165A

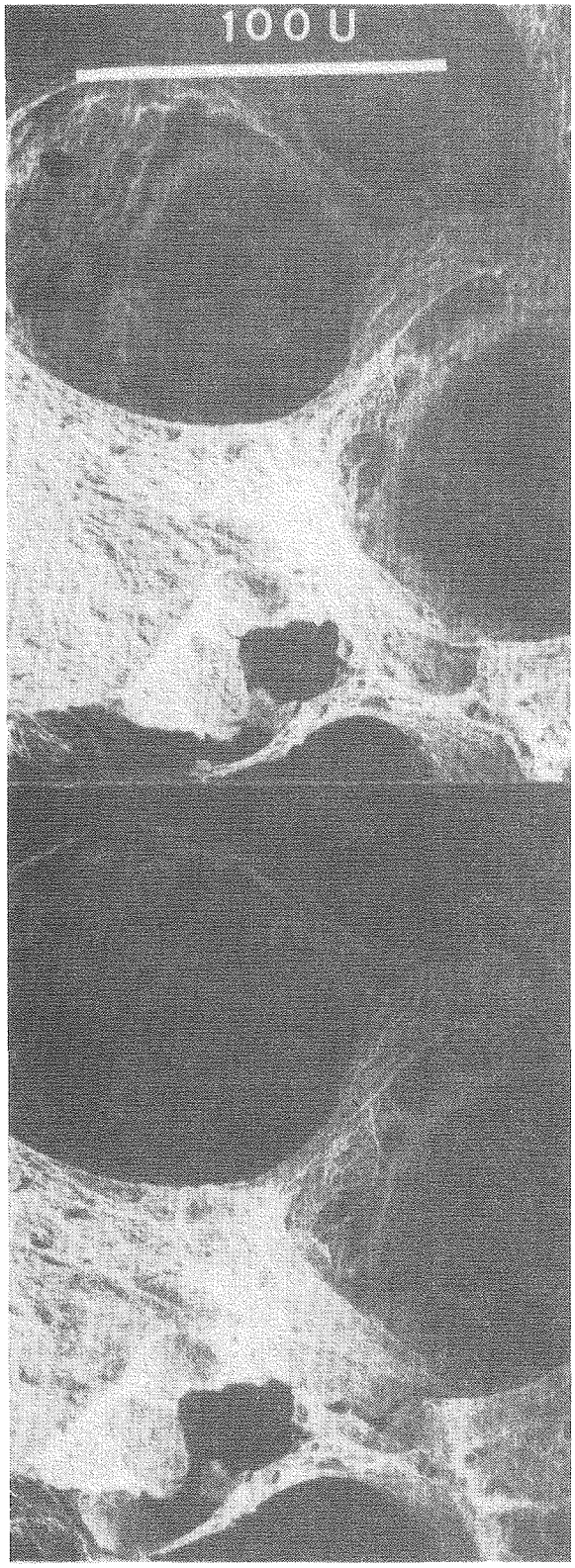

Figure 33. Same area as in Figure 31 but after warming the sample to -30°. Note the disappearance of the membrane structures across the alveoli.

XBB 800-13167A

Figure 34. Control lung stereopair SEM micrographs of lung prepared by airway perfusion of fixative, dehydrated critical point drying and metal coating (magnification 500X). XBB 800-31684A

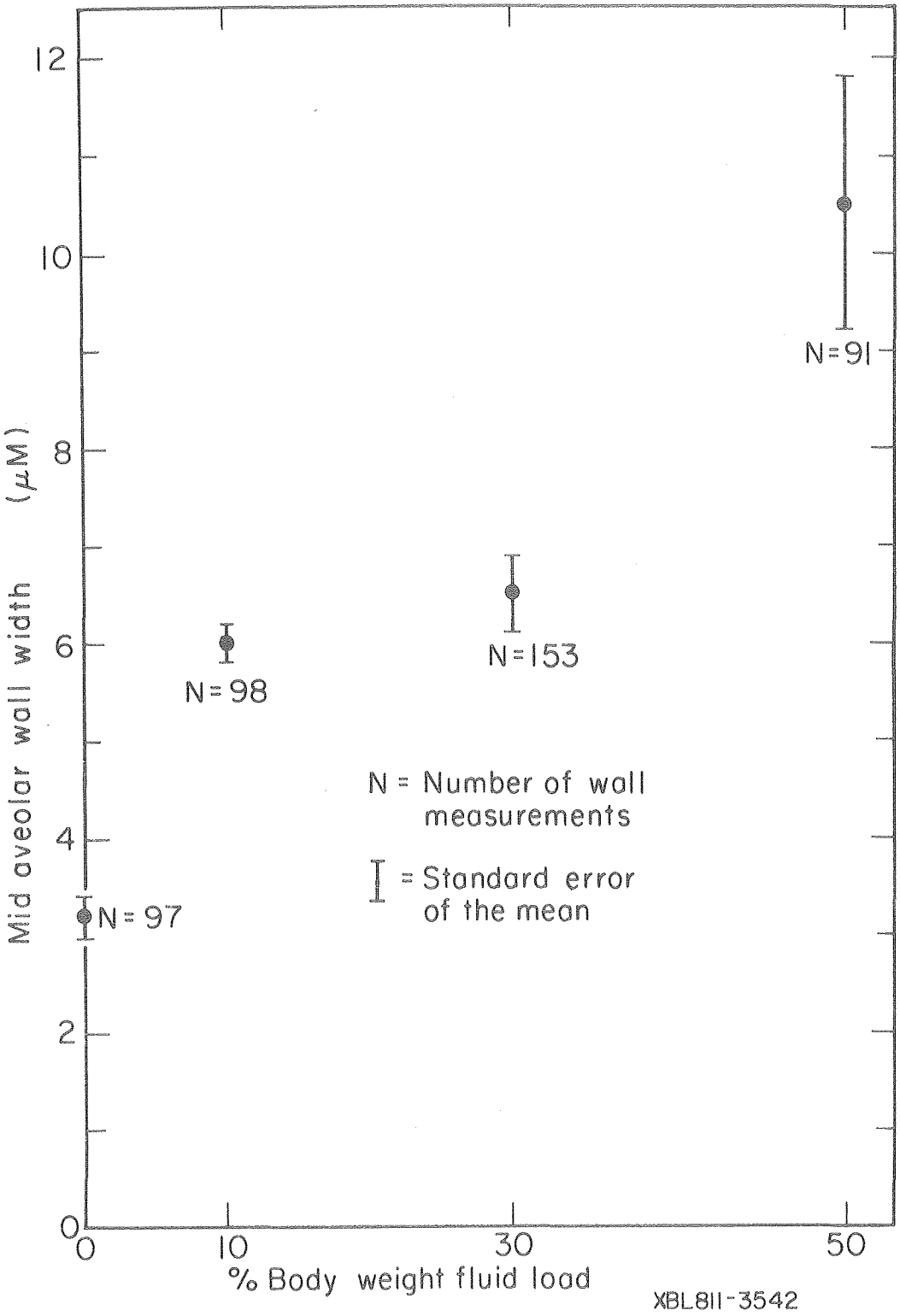

Figure 35. Mid alveolar wall width as a function of percent body weight fluid load.

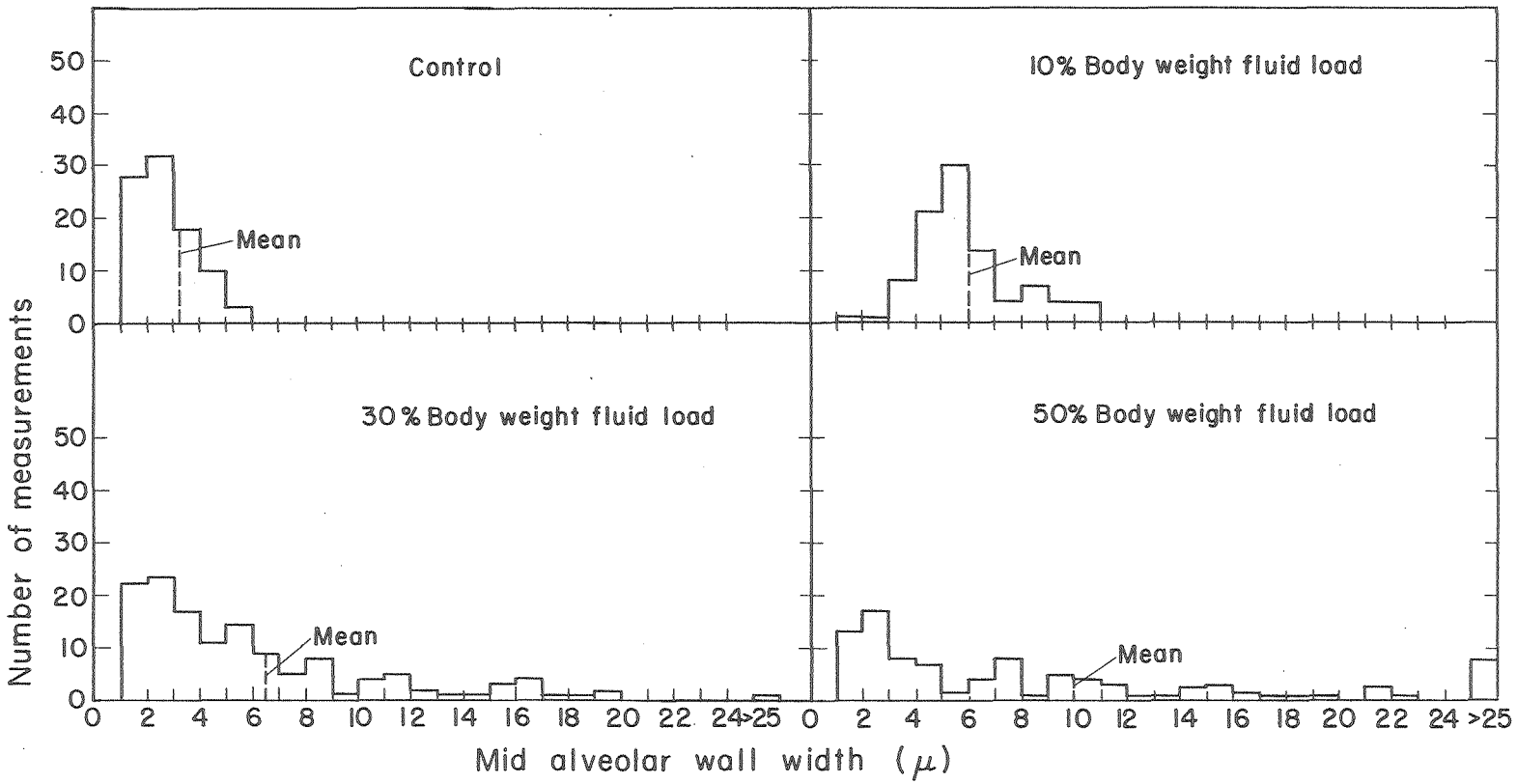

Figure 36. The distribution of mid alveolar wall width measurements for control 10, 30, and 50% body weight loads.

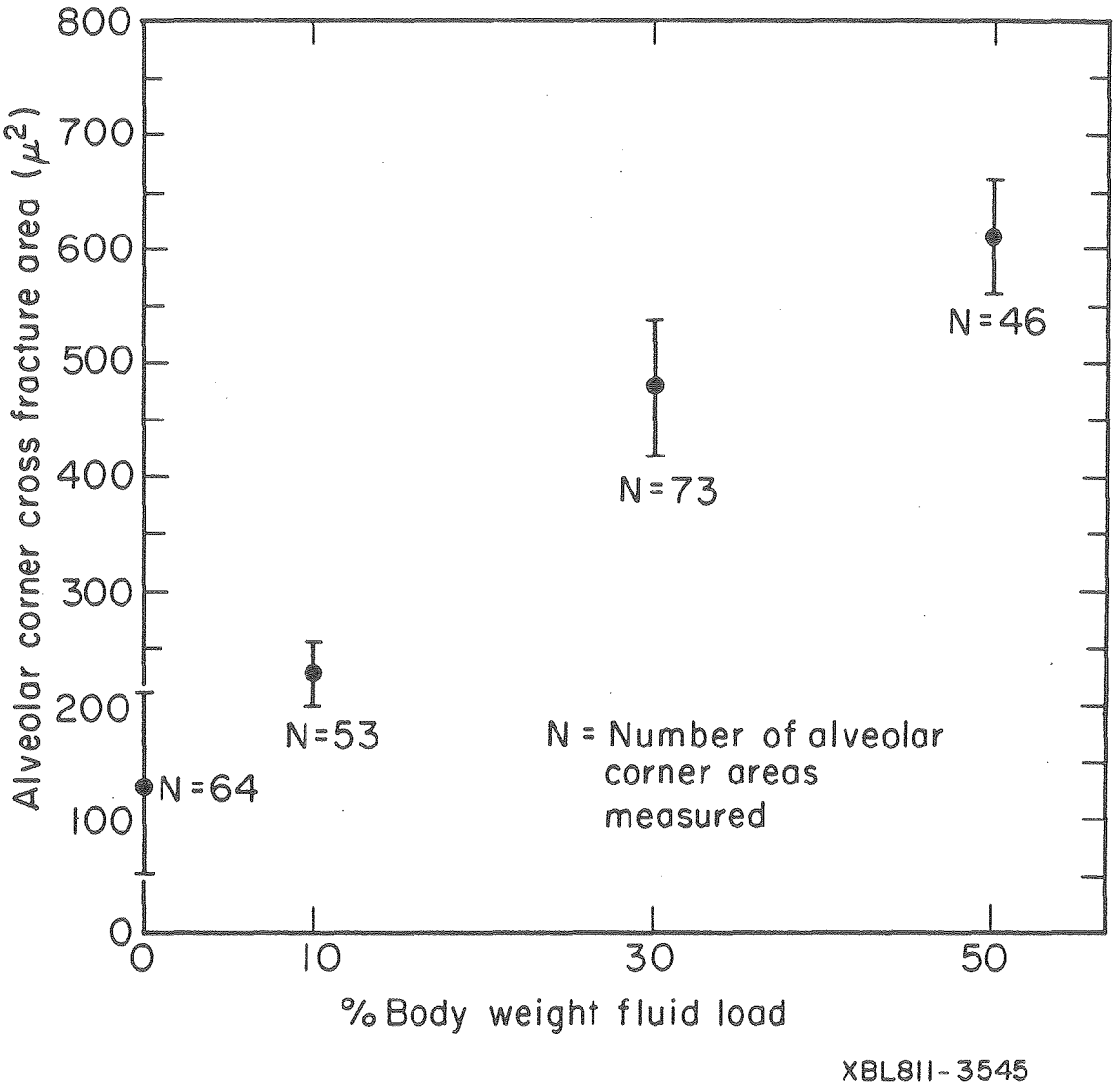

Figure 37. Alveolar cross fracture area as a function of percent body weight fluid load.

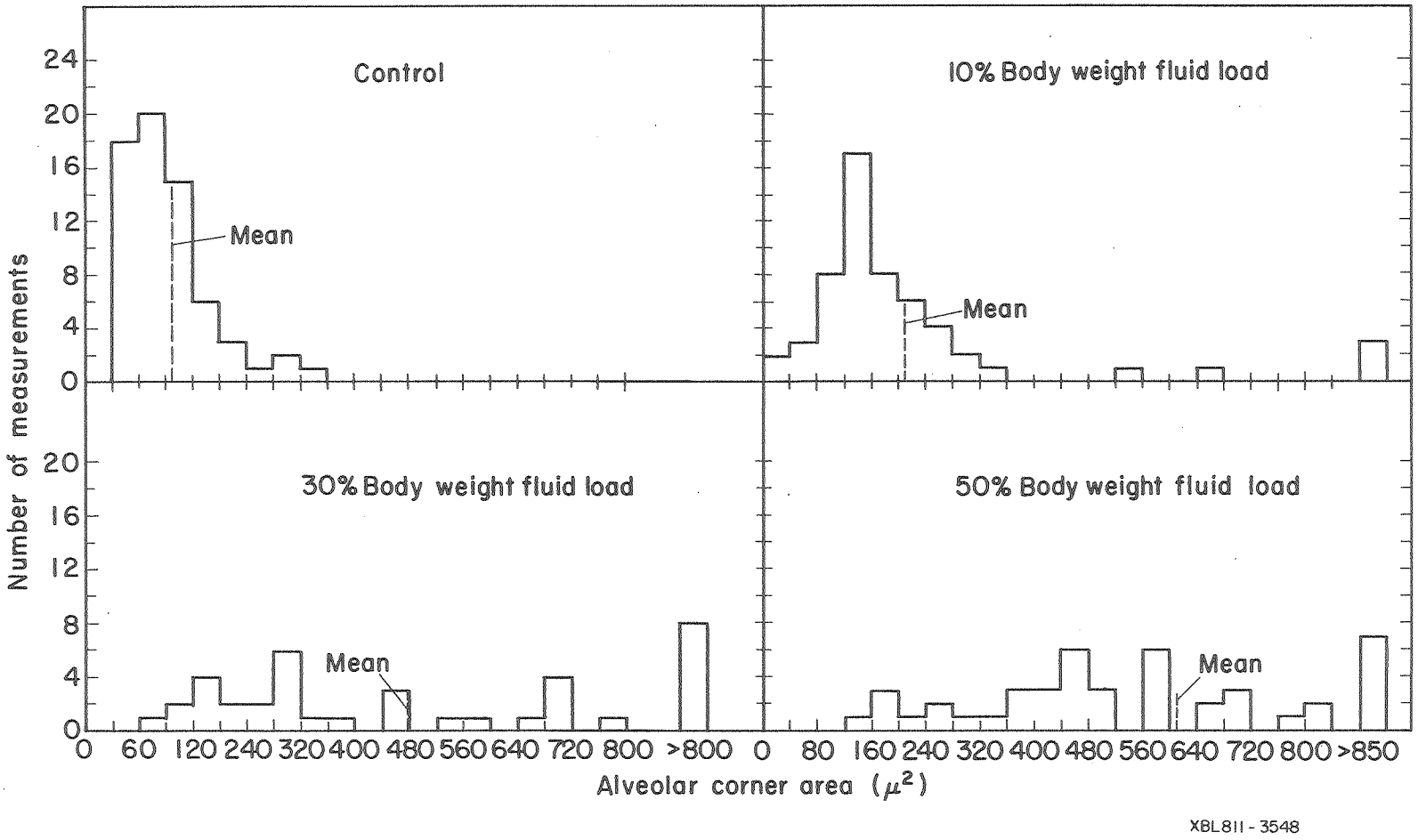

Figure 38. The distribution of alveolar corner area measurements for control 10, 30, and 50% body weight fluid loads.

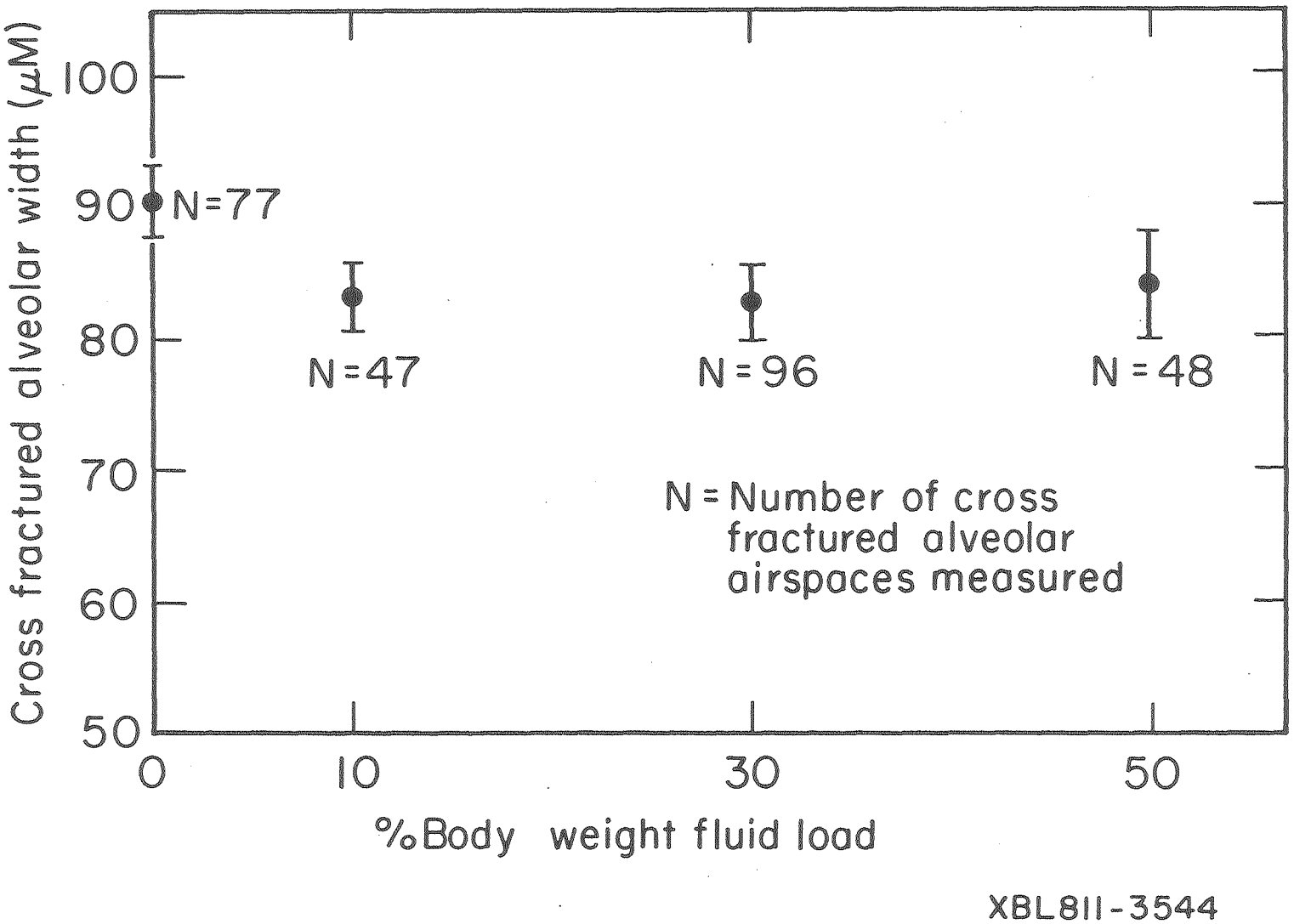

Figure 39. Alveolar width as a function of percent body weight fluid load.

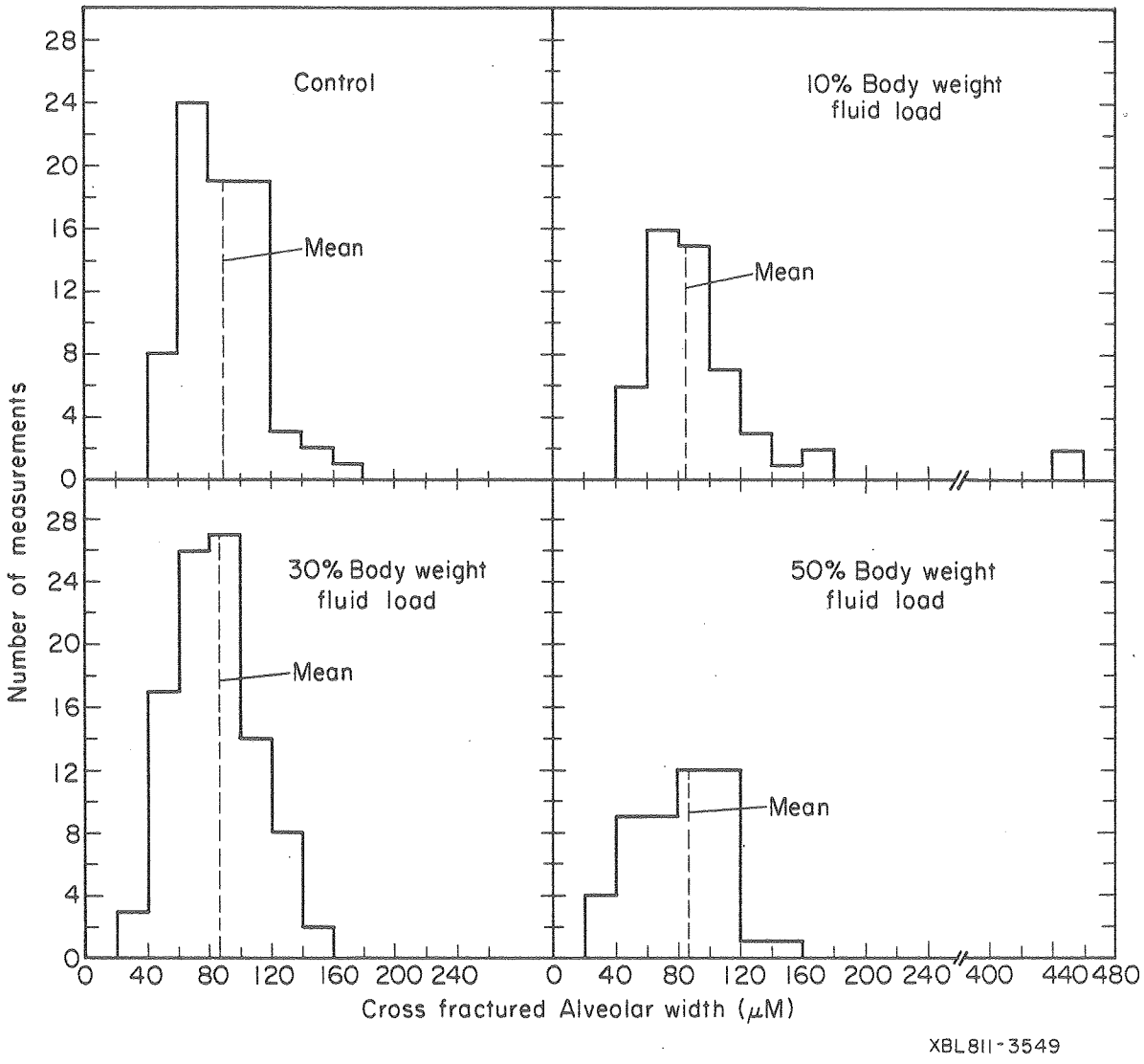

Figure 40. Distribution of alveolar width measurements for control, 10, 30 and 50% body weight.

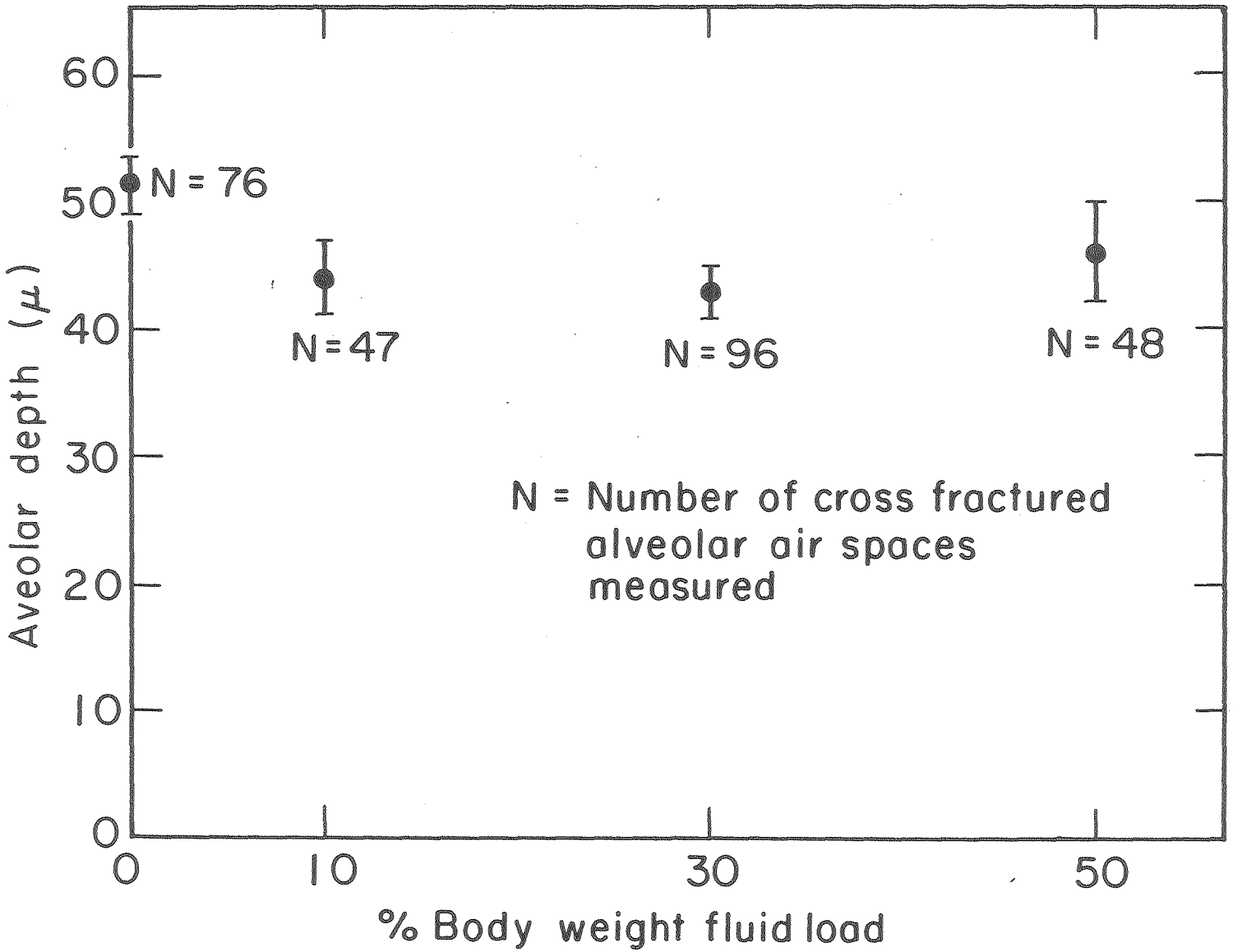

Figure 41. Alveolar depth as a function of percent body weight fluid load.

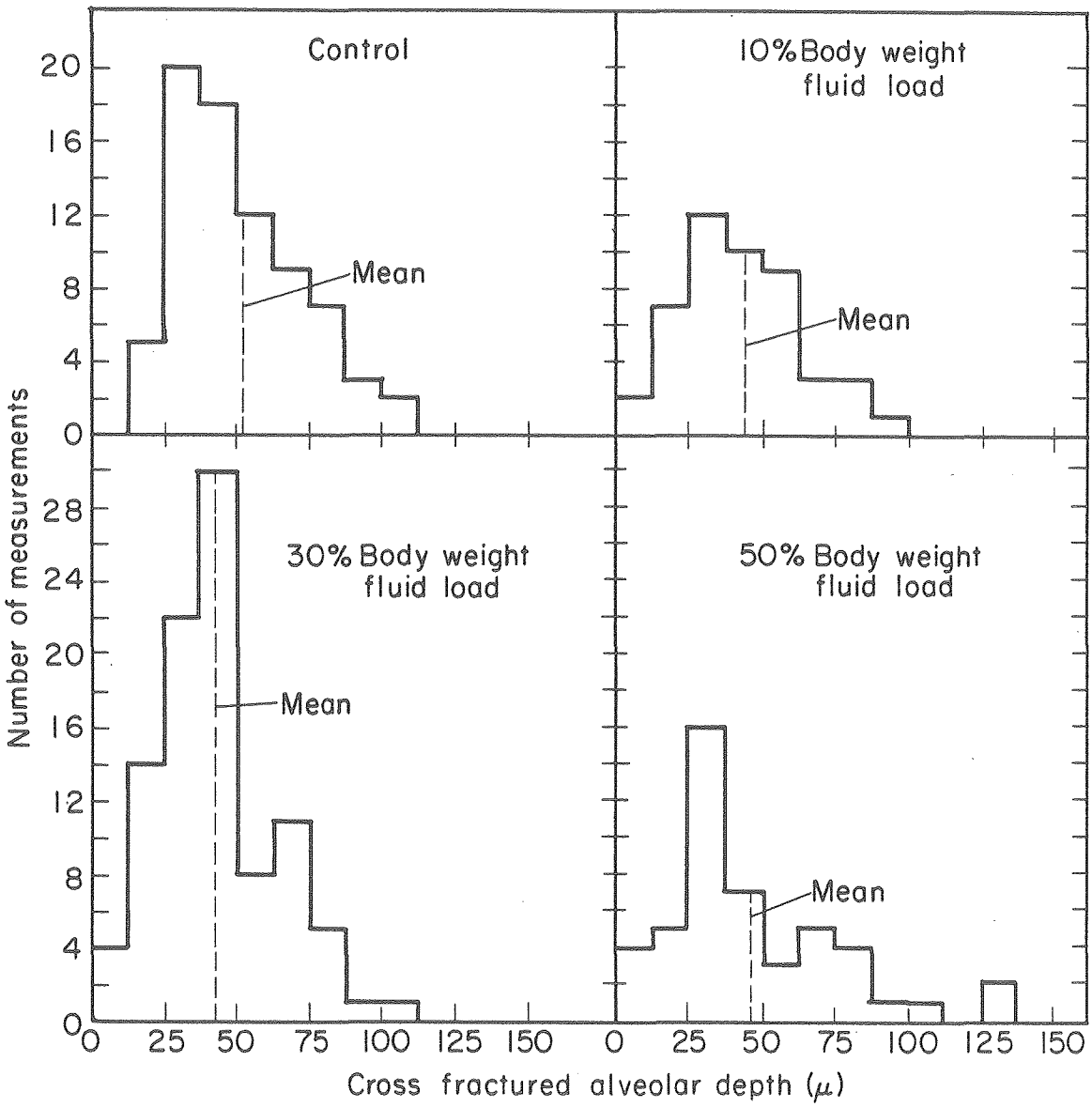

Figure 42. The distribution of alveolar depth for control 10, 30 and 50% weight fluid loads.

ALVEOLAR FLUID DISTRIBUTION RESULTING FROM
PROGRESSIVE HIGH PRESSURE PULMONARY EDEMA

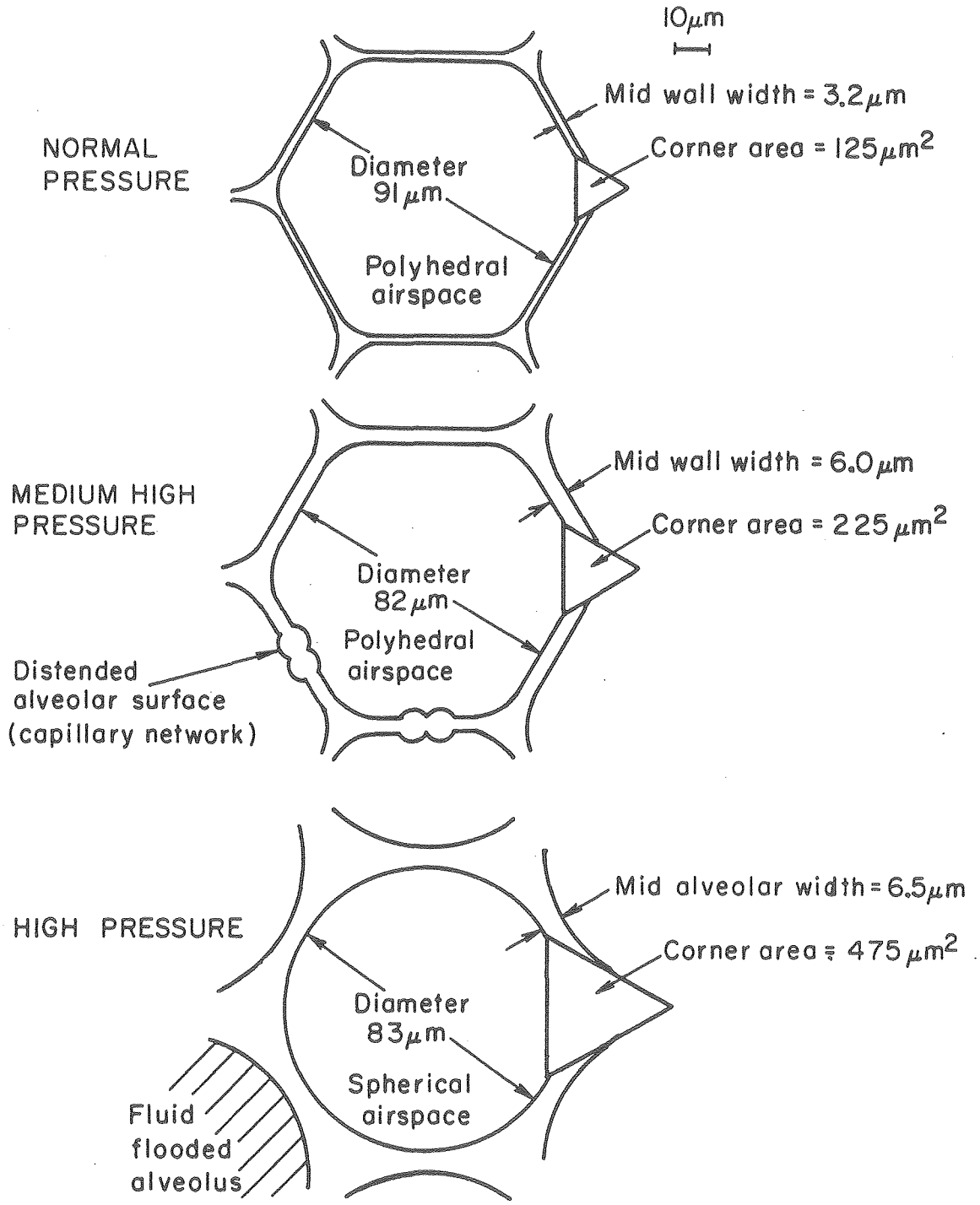

XBL811-3541

Figure 43. The model of alveolar dimensions resulting from progressive high pressure pulmonary edema.

REFERENCES

Bastacky, J., L. M. Sprague, and T. L. Hayes. Positional microstructure of the human lung: Microdissection and correlative microscopy techniques (LM, SEM, TEM), Proc. 38th EMSA Meeting, pp. 774-775, 1980.

Bhattacharya, J. and N. C. Staub. Direct measurement of microvascular pressure in the isolated, perfused dog lung. Microvasc. Res. 17 (Part 2): 586, 1979.

Boyde, A. Practical problems and methods in three dimensional analysis of SEM images. Scanning Electron Microscopy, 1970b, IITRI, Chicago, pp. 105-112.

Boyde, A. Quantitative Photogrammetric analysis and qualitative stereoscopic analysis of SEM images. Journal of Microscopy Vol. 98, Pt. 3, August 1973, pp. 452-471.

Boyde, A. Freeze, freeze-fracturing and freeze-drying in biological specimen preparation for SEM. Scanning Electron Microscopy/1974, IITRI, Chicago, pp. 1043-1046.

Boyde, A. Pros and cons of critical point drying and freeze-drying for SEM. Scanning Electron Microscopy/1978/Vol. II, SEM Inc., pp. 303-314.

Boyde A., E. Bailey, S. J. Jones, and A. Tamarin. Dimensional changes during specimen preparation for SEM. SEM/IITRI/1977, Vol. 1, pp. 507-518.

Branton, D. Fracture faces of frozen membranes. Proc. Nat. Acad. Sci., 55, 1048-1056, 1966.

Chase, W. H. The surface of pulmonary alveolar walls. Experimental Cell Research 18, 15-28, 1959.

Cotrell, T. S., Levine, O. R., Senior, R. M., Weiner, D., Spiro, D., and Fishman, A. P. Electron microscopic alterations at the alveolar level in pulmonary edema. Circ. Res. 21: 783-797, 1967.

DeFouw, D. O., and Berendsen, P. B. Morphological changes in isolated perfused dog lungs after acute hydrostatic edema. Circulation Res., Vol. 43, No. 1, 72-82, 1978.

DeFouw, D. O. and Berendsen, P. B. A morphometric analysis of isolated perfused dogs lungs after acute edema. Microvasc. Res. 17:90 1979.

Defouw, D. O. Morphological study of the alveolar septa in normal and edematous isolated dog lungs fixed by vascular perfusion. Lab. Investigtation, Vol. 42, No. 4, p. 413-419, 1980.

Echlin, P. Low temperature scanning electron microscopy: a review. J. of Microscopy Vol. 112, Pt. 1, pp. 47-61, 1978.

Fishman, A. P. Pulmonary edema. The water-extchanging function of the lung. Circulation 46: 390-408, 1972.

Fishman, A. and G. G. Pietra. Hemodynamic pulmonary edema in Pulmonary Edema. eds. A. P. Fishman and E. M. Renkin, American Physiological Society, pp. 79-96, 1979.

Franks, F. Biological freezing and cryofixation. J. of Microscopy, Vol. III, Pt. 1, p. 3-16, 1977.

Fujikawa, S. and T. Nei. A technique for observing the three-dimensional structure of erythrocytes with a cryoscanning electron microscope. J. Electron Micros., Vol. 27, No. 1, pp. 55-58, 1978.

Gaar, R. A., A. E. Taylor, L. J. Owens et al. Pulmonary capillary pressure and filtration coefficient in the isolated perfused lung. Am. J. Physiol. 213: 910-914, 1967.

Gee, M. H. and D. O. Willaism. Effect of lung inflation on pre-vascular cuff fluid volume in isolated dog lobes. Microvascular Res. 17, 192-201, 1979.

Gehr, P. and E. R. Weibel. Morphometric estimation of regional differences in the dog lung. J. Appl. Physiol. 37: 648-653, 1974.

Gehr, P., M. Bachofen, and E. R. Weibel. The normal human lung: ultrastructure and morphometric estimation of diffusion capacity. Respiration Physiol. 32:121-140, 1978.

Gil, J. Morphologic aspects of alveolar microcirculation. Federation Proc. 37: 2462-2465, 1978.

Gil, J. and E. R. Weibel. Improvements in demonstration of lining layer of lung alveoli by electron microscopy. Res. p. Physol. 8:13-36, 1969/70.

Greene, D. G. Pulmonary edema in Handbook of Physiology Sect. 3 Respiration, Vol. II, eds. W. O. Fenn and H Rahn, American Physiological Society, pp. 1585-1600, 1965.

Groniowski, J. and M. Walski. Cryo-scanning electron microscopy of the lungs. Annals. Med. Sect. Pol. Acad. Sci., Vol. 19, No. 2, pp. 107-108, 1974.

Grossmann, G. Histological evaluation of lung expansion in relation to various fixation techniques-immersion, perfusion and rapid freezing. Acta Path. Microbiol. Scand. Sect., A, 892, 582-585, 1974.

Guyton, A. C. and Lindsey, A. W. Effect of elevated left artial pressure and decreased plasma protein concentration on the development of pulmonary edema. Circulation REs. 7: 640-657, 1959.

Hayes, T. Biophysical aspects of scanning electron microscopy. Scanning Electron Microscopy/1980/I SEM Inc., Chicago, pp. 1-10.

Hogg, J. G., J. B. Agarawal, A. J. S. Gardiner, W. H. Palmer, and P. T. Macklem. Distribution of airway resistance with developing pulmonary edema in dogs. J. Appl. Physiol. 32(1): 20-24, 1972.

Hook, G. and C. Schooley. Freeze-fracture replicas produced in the scanning electron microscope. J. Cell Biol. 79, 2, 1616 (1978).

Henry, R. J. Chemical Chemistry, Principles and Techniques. New York: Harper and Row, p. 179-184, 742-744 1964.

Heuser, J. E., T. S. Reese, M. J. Dennis, Y. Jan, L. Jan, and L. Evans. Synaptic vesicle exocytosis captured by quick freezing and correlated with quantal transmitter release. J. Cell Bio. Vol. 81, 275-300, 1979.

Howell, P.G.T. A theoretical approach to the errors in SEM photogrammetry. Scanning Vol. 1, 118-124, 1978.

Howell, P. G. Stereometry as an aid to stereological analysis. J. Microscopy, Vol. 118, Pt. 2, pp. 217-220, 1980.

Hughes, J.M.B., J. B. Glazier, T. E. Maloney, and J. B. West. Effect of extra-alveolar vessels on distribution of blood flow in the dog lung. J. Appl. Physiol. 29, 332-339, 1970.

Inoue, S., R. P. Michel, and J. C. Hogg. Zonulae Occludentes in alveolar epithelium and capillary endothelium of dog lungs studied with the freeze-fracture technique. J. of Ultrastructural REs. 56, 215-225, 1976.

Iliff, L. D. Extra-alveolar vessels and edema development in excised dog lungs. Circulation Res. 28: 524-532, 1971.

Kistler, J. and E. Kellenberger. Collapse phenomena in freeze-drying. J. of Ultrastructure Research 59, pp. 70-75, 1977.

Landis, E. M. and J. R. Pappenheimer. Exchange of substances through the capillary walls in Handbook of Physiology. Circulation, Washington D.C. Am. Physiol. Soc., Sect 2., vol. II, pp. 961-1034, 1963.

Levine, O. R., R. B. Mellins, R. M. Senior, and Fishman. The application of Starling's law of capillary exchange to lungs. J. Clin. Invest. 46: 934-944, 1967.

Mazzone, R. W., S. Kornblau, and C. M. Durand. Shrinkage of lung after chemical fixation for analysis of pulmonary structure-function relations. J. Appl. Physiol. 48(2): 382-385, 1980.

Mazzone, R. W., C. M. Durand, and J. B. West. Electron microscopy of lung rapidly frozen under controlled physiological conditions. J. Appl. Physiol: 42(2):325-333, 1978.

Mazzone, R. W., C. M. Durand, and J. B. West. Electron microscopic appearances of rapidly frozen lung. J. of Microscopy, Vol. 117, Pt. 2, pp. 269-284, 1979.

Moor, H., and Muhlenthaler, K. Fine structure in frozen-etched yeast cells. J. Cell Biology 17, 609-628, 1963.

Muir, A. L., D. L. Hall, P. Despas, and J. C. Hogg. Distribution of blood flow in lungs in acute pulmonary edema in dogs. J. Appl. Physiol. 33: 763-769, 1972.

Nermut, M. V. Freeze-drying for electron microscopy in, Principles and Practice of Electron Microscopy, ed., Hayat, Vol. 7, pp. 79-117.

Nowell, J. and W. Tyler. Scanning electron microscopy of the surface morphology of mammalian lungs. American Review of Respiratory Disease, Vol. 103, 1971, pp. 313-328.

Parra, S. C., L. R. Gaddy, and T. Takaro. Ultrastructural studies of canine interalveolar Pores (Of Kohn). Laboreatory Investigation, Vol. 38, No. 1, p. 8-13, 1978.

Pawley, J., T. L. Hayes, and G. Hook. Preliminary studies of coated complementary freeze-fractured yeast membranes viewed directly in the SEM. Scanning Electron Microscopy/1978/Vol. 11, Chicago, pp. 613-684.

Pawley, J. B. and J. T. Norton. A chamber attached to the SEM for fracturing and coating frozen biological samples. J. Microscopy 112, 1978.

Pawley, J. B., G. Hook, T. L. Hayes, and C. Lai. Direct scanning electron microscopy of frozen-hydrated yeast. Scanning, Vol. 3, No. 3, pp. 219-226, 1980.

Pearce, M. L., J. Yamashita, and J. Beazell. Measurement of pulmonary edema. Circulation Res. 16: 482-488, 1965.

Pietra, G. G., J. P. Szidon, and A. P. Fishman. Leaky pulmonary vessels. Trans. Assoc. Am. Physicians 85: 369-376, 1972.

Plopper, C. G., D. L. Dungworth, and W. Tyler. Pulmonary Lesions in Rats Exposed to Ozone, A correlated light and electron microscopic study. Amer. J. of Pathology, Vol. 71, No. 3, pp. 375-398, 1973.

Renkin, E. Miltiple pathways of capillary permeability, Circulation Res. 41: 735-743, 1977.

Rusznyak, J., M. Foldi, and G. Szabo. Lymphatics and Lymph Circulation Physiology and Pathology (2nd ed.) Oxford: Pergamon, 1967, 971 p.

Robin, E. D., Cross, C. E, and Zelis, R. Pulmonary edema. N. Eng. J. Med. 288:239-246, 1973.

Said, S. I., J. W. Longacher, Jr., R. K. Davis, C. M. Baneajee, W. M. Davis, and W. J. Woodell. Pulmonary gas exchange during induction of pulmonary edema in anesthetized dogs. J. Appl. Physiol. 19:403-407, 1964.

Schafer, V., H. Hucker, and K. Meinen. Early morphological alterations of the rat lung with increased intracranical pressure. Res. Exp. Med. 165, 1-8, 1975.

Schneeberger, E. E. Structural basis for some permeability properties of the air-blood barrier. Federation Proc. 37:3471-2478, 1978.

Schneeberger-Keeley, E. E., and M. J. Karnofsky. The ultrasturctural basis of alveolar-capillary membrane permeability to peroxidase used as a tracer. J. of Cell Bio., Vol. 37, 781-793, 1968.

Selinger, S. L., R. D. Bland, R. H. Demling, and N. C. Staub. Distribution volumes of [^{131}I] albumin, [^{14}C] surcrose and ^{36}Cl in sheep lung. J. Appl. Physiol. 39(5): 773-779, 1975.

Sharp, J. T., G. T. Griffith, I. L. Bunnell, and D. G. Greene. Ventilatory mechanics in pulmonary edema in man. J. Clin. Invest. 37:111-117, 1958.

Simionescu, M., N. Simionescu, G. E. Palade. Permeability of muscle capillaries to small hemepeptides. Evidence for the existence of patent transendothelial channels. J. Cell. Biol. 64: 586-607, 1975.

Snashall, P. D., Weidner, W. J., and Staub, N. C. Extravascular lung water after extracellular fluid volume expansion in dogs. J. of Applied Physiology, Vol. 42, No. 4, April, 1977.

Starling, E. H. On the absorption of fluids from the connective tissue spaces. J. Physiol., London 19: 312-326, 1896.

Staub, N. C. Pulmonary edema, Physiol. Rev. Vol. 54, No. 3., pp. 678-811, 1974.

Staub, N. C. Pulmonary edema due to increased micjrovascular permeability to fluid and proteins. Circ. Res. 43:143-151, 1978.

Staub, N. C. Pulmonary edema. Physiologic approaches to management. Chest 74:559-564, 1978.

Staub, N. C. Pathways for fluid and solute fluxes in pulmonary edema in Pulmonary Edema, eds. A. P. Fishman, and E. M. Renkin, American Physiological Society, pp. 113-124, 1979.

Staub, N. C. The pathogenesis of Pulmonary edema. Progress in Cardiovascular Research, Vol. XXIII, No. 1 (July/August), 1980.

Staub, N. C., H. Nagano and N. L. Pearce. Pulmonary edema in dogs, especially the sequence of fluid accumulation in lungs. J. Appl. Physiol. 22:227-240, 1967.

Storey, W. F. and N. C. Staub. Ventilation of terminal air units. J. Appl. Physiol. 17(3):391-397, 1962.

Southworth, D., K. Kisher, and D. Branton. Principles of freeze-fracturing and ethcing in Techniques of Biochemical and Biophysical Morphology, Vol. 2, Ed., D Glick and R. M. Rosenbaum, Publ. John Wiley and Sons, N.Y., pp. 247-281, 1975.

Takaro, T., P. Price, S. Paraa, and L. R. Gaddy. Ultrastructural studies of aperatures in the interalveolar septums of the adult human lung. Am. Review of Resp. Disease, Vol. 119, 425-435, 1979.

Untersee, P., J. Gil., and E. R. Weibel. Visualization of extra cellular lining layer of lung alveoli by freeze-etching. Respiration Physiology 13, 171-185, 1971.

Visscher, M. B., F. J. Haddy, and G. Stephens. The physiology and pharmocology of lung edema. Pharmacol. Rev. 8:389-434, 1956.

Vreim, C. E. and N. C. Staub. Protein composition of lung fluids in acute alloxan edema in dogs. Am. J. Physiol. 230: 376-379, 1976.

Vreim, C. E., P. D. Snashall, and N. C. Staub. Protein composition of lung fluids in anesthetized dogs with acute cardiogenic edema. Am. J. Physiol. 231: 1466-1469, 1976.

Wang, N. S. and Ying, W. L. A scanning electron microscopic study of alkali-digested human and rabbit alveoli. Am. Rev. Respirat. Disease 115:449-460, 1977.

Weibel, E. R. and B. W. Knight. Morphometric study on the thickness of the pulmonary air-blood barrier. J. of Cell Biology, Vol. 21, pp. 367-384, 1964.

Weibel, E. R., and J. Gil. Electron microscopic demonstration of an extracellular duplex lining layer of alveoli. Respiration Physiol. 4: 42-57, 1968.

Weibel, E. R. and Gil, J. Structure-function relationships at the alveolar level. In: Bioengineering Aspects of the Lung, edited by J. B. West, New York: Dekker, 1977, p. 1-81.

West, J. B., C. T. Dollery, and B. E. Heard. Increased pulmonary vascular resistance in the dependent zone of the isolated dog lung caused by perivascular edema. Circulation Res. 17: 191-206, 1965.

Woolverton, W. C., K. L. Brigham, and N. C. Staub. Effect of positive pressure breathing on lung lymph flow and water content in sheep. Circulation Res. 42: 550-557, 1978.

APPENDIX C

Stereo Observation of Low Temperature SEM Micrographs

Optical stereo information can be obtained when the same object is viewed from two directions. Most people see with two eyes and the interocoular distance is such that objects held within arm's reach appear in stereo. Stereo effect in the SEM is achieved by photographing the same sample area at two tilt positions and observing each photograph separately in each eye. To separate convergence and focus so that one eye sees one micrograph, it is convenient to use an optical viewer. The Nesh System Stereo glasses (Suedstrib, P. O. B. 5726, D-4400, Muerster, W. Germany) optically separates vertically mounted stereopair micrographs with prisms directing the high/low micrographs into the right/left eyes. The micrographs were mounted so that the y axis of tilt is in the verticle direction.

Instructions on Stereopair Micrograph Observation Using Stereo Glasses

Nesh system stereo glasses are included with the Dissertation (located on back cover). To see the stereo effect, hold the glasses to the eyes with the right hand with the nose notch down and hold the dissertation with the left hand (in the normal reading orientation). Three images should be seen; upper, middle, and lower. When the stereo pair micrographs are in verticle registry, the middle image is composed of the two superimposed images and is in stereo. The distance from the viewer to the stereomicrographs determines the verticle seperation of the stereo pairs and it is this distance that is adjusted in order to view stereo. For the SEM micrographs presented here, verticle registry

is achieved by holding the glasses 30 cm from the stereo pairs which is the approximate length of the chord used to attach the glasses to the Dissertation. Exact verticle registry can be obtained by moving the glass in small increments toward or away from the micrographs.